ROBUST PERIODIC DISTURBANCE COMPENSATION VIA MULTIRATE CONTROL

CHANG DUAN

NATIONAL UNIVERSITY OF SINGAPORE

2005

Robust Periodic Disturbance Compensation via Multirate Control

CHANG DUAN

(B.Eng.(Hons.), HUST)

A THESIS SUBMITTED

FOR THE DEGREE OF MASTER OF ENGINEERING

DEPARTMENT OF ELECTRICAL & COMPUTER ENGINEERING

NATIONAL UNIVERSITY OF SINGAPORE

2005

Acknowledgments

First of all, I would like to thank Professor Chong Tow Chong for his guidance and concern through the period of my study in Data Storage Institute (DSI). I also wish to thank Dr. Guoxiao Guo, my research supervisor, for giving me valuable advices on my research work and influencing my way of thinking. He taught me how to do research effectively. He also encouraged me to take part in academic activities through which I was inspired by other researchers and gain a lot of academic knowledge.

I appreciate colleagues and former colleagues Mr JingLiang Zhang, Dr. Lu Feng, Ms Wai Ee Wong, Dr. ChunLing Du and Dr. RuiFeng Chen for their consultation and advices.

Thanks also go to Mr. Jinchuan Zheng and Mr. Chee Khiang Pang, two of Ph.D candidates supervised by Dr. Guo in Mechatronics and Recording Channel (MRC) division. I always discuss issues I encountered in control theory and experiments with them. Their experiences and ardent suggestion helped me a lot.

Last but not least, I would like to express my deepest gratitude to my parents for their continuous love and moral support given to me.

Contents

Summary

Today, it is pretty hard for us to image what the world would look like without computer and what computer would be like without hard disk drives (HDDs) [22]. Areal densities of hard disk drives (HDDs) have exceeded 100 $Gb/inch^2$ in the year 2004. Since a higher track density, and thus a higher areal density, can only be achieved through a reduction in absolute track misregistration (TMR), the influence of high frequency disturbances become more significant. To achieve a higher TPI number, various vibrations and disturbances need to be reduced either via mechanical design or suppressed by higher bandwidth servos that have higher levels of disturbance rejection.

As one of the prospective control applications, multirate control has the advantage of more flexibility (by using different sampling rate for reference signal, control signal and output signal) in design and thus possibility for better performance. When applied to the disk drive servo system, generally a better transient and steady state performance is expected.

This thesis deals with control schemes based on multirate control theory which are designed to cancel periodic disturbance. The following issues are discussed in this thesis:

(i) A plant inverse method based on multirate discretizationis is applied to Repeatable Runout (RRO) compensation. The method differs from previous method, the so-called zero phase inverse method, in which different schemes are used to design for minimum phase plant and non-minimum phase plant. With this conventional method, the zero phase can not be assured when the plant is of non-minimum phase. With the proposed multirate Adaptive Feedforward Compensation (AFC) scheme, we can shape the plant to be of zero phase over wide frequency range no matter the plant is of minimum phase or not.

(ii) To further improve the control system performance against disturbance that can be treated as periodic disturbance, including RRO and some external Non-Repeatable Ruout (NRRO), an adaptive feedforward compensator based on the proposed plant inverse scheme is proposed. The proposed scheme attenuates the RRO components over a wide frequency range without amplifying other frequencies; in contrast, unselected RRO components may be amplified using the conventional AFC scheme.

(iii) An application example of applying the proposed scheme to spin stand servo system is given. Simulation and experiment results have confirmed the analysis results above, and also shown that the proposed scheme can reduce the PES signal more rapidly even when the disturbance signal is a time-varying one. The scheme is also robust against plant parameter variations.

As the areal density of the HDDs continuously grows and there is not yet a high capacity and a high transfer rate alternative product to replace the HDDs, the future research work will continue to be focused on obtaining a better PES, higher bandwidth actuator design and more effective servo control algorithms to attenuate vibrations, which are discussed in future work part.

Nomenclature

Unless otherwise specified, the following abbreviations and symbols are used throughout this dissertation.

AFC:	Adaptive Feedforward (Runout) Compensation,
BPI:	Bits Per Inch,
FFT:	Fast Fourier Transform,
HDA:	Head Disk Assembly,
HDD:	Hard Disk Drive,
LDV:	Laser Doppler Vibrometer,
LQG:	Linear Quadratic Gaussian,
LQR:	Linear Quadratic Regulator,
MIMO:	Multi-Input Multi-Output,
NRRO:	Non Repeatable Runout,
PES:	Position Error Signal,
PID:	Proportional, Integral and Derivative,
RHP:	Right Half Plane,
RPM:	Revolutions Per Minute,
RRO:	Repeatable Runout,

SISO: Single-Input Single-Output,

TMR: Track Mis-Registration,

TPI: Track Per Inch,

List of Figures

Chapter 1

Introduction

The magnetic hard disk drives (HDDs) are high precision and high performance mechatronic devices which are produced in very high volumes and are sold at low price. Since the first HDD was introduced in 1956, this device has been the recipient of significant additional technology innovations which have extended its value. In this chapter, the trends and challenges of HDD technology and the background of the research work are presented.

1.1 Trends and Challenges of Disk Drive Technology

Fig. 1.1 shows a schematic of a hard disk drive, in which the components are identified. The storage medium is a thin-film magnetic material deposited on a glass or aluminum substrate. The magnetic material is protected by an overcoat to prevent corrosion and a lubricant to protect against wear. The circular disk is mounted on a spindle with high precision ball bearings or fluid bearings. The basic magnetic storage phenomenon occurs when a read/write sensor (head) scans the rotation disk surface. At specific concentric rings (tracks), magnetized regions are created in a write operation, or read if previously written. Precision mechanical systems support this scanning process. A miniature motor buried within the spindle of the disk and an actuator motor operating on a voice-coil principle position the head over the disk. A ramp assembly allows the head to fly aerodynamically over the disk surface during periods of disk rotation, promoting the use of ultra-smooth disks which enable low flying, resulting in a higher data density. Magnetic impulses during the read operation are converted to analog electrical signals by an amplifier and eventually are decoded and error-corrected by a data channel. The electronics content of HDDs is large enough to perform this data function as well as to control each operation and drive the mechanical assemblies [48].

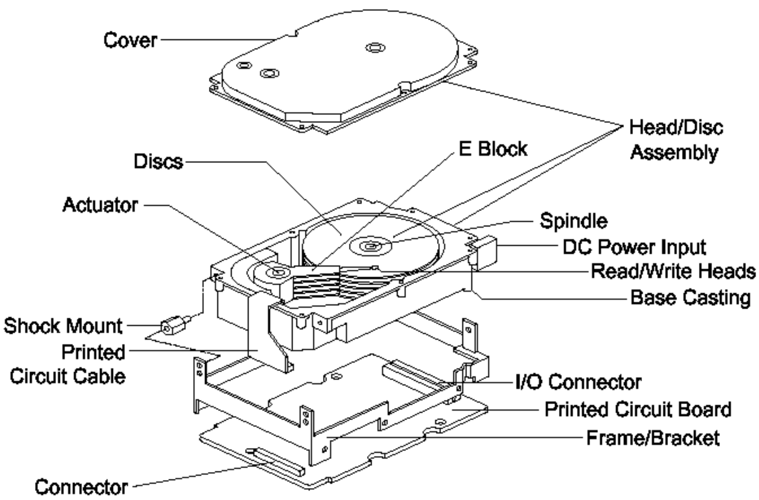

Figure 1.1: A typical hard disk drive.

An obvious evolution direction is the significant reduction of disk size and increase of data storage densities, faster data transfer rate and shorter data access time, reduction of production cost and application to mobile devices and consumer electronic products [71].

1) Smaller form factor.

Since the 1980's, smaller form factor drives have grown in storage capacity. As of 2004, 3.5 inch form factor drives designed for the server market can store more than 146 Gbytes in a 1 inch height using 84 mm diameter disks rotating at 10,000 RPM, desktop drives can store 250 Gbytes per drive on 95 mm diameter disks rotating at 7200 RPM, 2.5 inch drives designed for mobile, notebook computers (and some compact desktop computers) can store 80 Gbytes on 65 mm disks rotating at power efficient 4200 RPM. A new form factor, 1 inch, the Hitachi GST Microdrive can store 1 Gbyte today with a projection of 4 Gbytes in the near future. Microdrive is designed for such consumer applications as digital cameras, personal communications devices and hand held computers. Form factor evolution to smaller sizes has been accomplished without loss of capacity and often has resulted in higher performance and lower power consumption.

2) Larger areal density.

A measurement of data storage density is the areal density, in bits per square inch, which is computed as the track density TPI (Track Per Inch) multiplied by the linear density BPI (Bit Per Inch) on each track. Since 1991, the rate of increase has accelerated to 60% per year, and since 1997 this rate has further accelerated to an incredible 100% per year. This acceleration is the result of the introduction of MR (magnetoresistive) read heads in 1991, GMR (giant magnetoresistive) read heads in 1997 and AFC (antiferromagnetically coupled) media in 2001. It is of interest to consider future areal density growth and the technology requirements to maintain this growth. Generally, the industry expects areal density to continue to increase to 100 Gbits/in^2 and beyond but at a somewhat lower growth rate.

Since 1997, track densities have been increasing faster than linear densities, one principal factor for the continuing increase in areal density. This trend is the result of improved read/write head designs that allow writing narrow tracks and reading information with adequate signal amplitude. Also, the trend is the result of precise track following based on advanced actuator mechanical designs and improved servo technologies. It was announced on Aug 4, 2004 that Toshiba has set a new benchmark for areal density in the 1.8-inch HDD category at 93.5 Gbits/in^2. This has allowed Toshiba to pack 30 GB of data onto a single 1.8-inch platter, an increase of 50 percent over current models, delivering drives that are ideally suited for in-demand consumer electronics products such as mobile audio players and mobile notebook PCs.

3) Lower cost.

The price per megabyte of disk storage has been decreasing at about 40% per year based on improvements in data density, – even faster than the price decline for flash memory chips. Recent trends in HDD price per megabyte show an even steeper reduction, 50% per year, making magnetic disk drives even more attractive as a storage technology. When considering the continuing price decline of DRAM and Flash memory chips, it is at least 10 times cheaper to store information with magnetic hard disk drives when compared with semiconductor memories. This lower price per megabyte of storage also make the 1 inch microdrive a competitive alternative to flash in digital cameras as well as other consumer based applications.

4) Mobile devices and consumer electronic products.

It has been reported that the increase rate of consumer electronic products is 43% CGR now. That indicates mobile devices and consumer electronic products have become and will continue to be big drivers of storage growth. Storage for digital camera, handphone, mp3 player, GPS navigation system, automobile computers, wearable computers and so on provide a high potential market for HDD applications. The moves to 3.5-,and 2.5-in disks (and smaller) have continued to allow more advanced manufacturing methods, smoother surfaces, lower power dissipation, lower flying heights and higher bit densities. Typical hard disk diameters are 3.5-in for desktop computers, 3-in and smaller for high-speed video and server applications, 2.5-in for laptop computers, and 1.8 or 1-in for PDAs and other mobile applications such as mp3 players [4].

5) Others

In addition to the increase of the disk areal density, the performance of disk drives such as average seeking time, data transfer rate has been improved considerably as well due to the improved technologies applied in the servo mechanic systems as well as electronics such as the higher disk rotational speed.

1.2 Challenges of Servo Control for Disk Drives

The improvement of disk drives technology requires the evolutionary developments of head, medium and servomechanism technologies. The servomechanism technology provides a means for moving a set of read/write heads to a fixed radial locations over the disk surface and maintaining the heads over the center of the track. Servo system performance is getting more emphasis because improving servo system in current hard disk drives (HDDs) is cost effective in achieving higher HDD density [4].

1.2.1 Introduction of Servo System in HDD

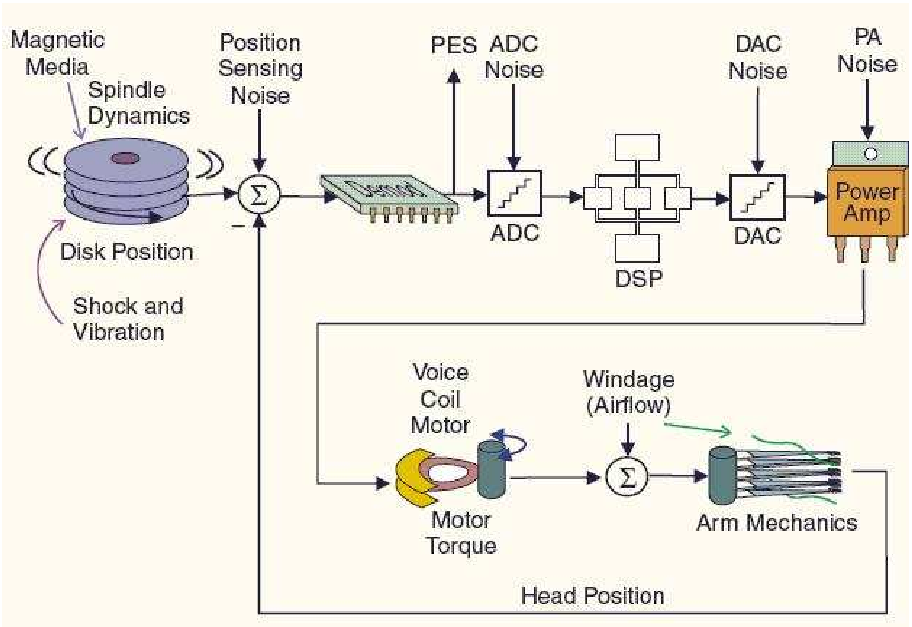

Figure 1.2: Generalized view of track-following model [4].

A schematic block diagram of a disk drive servo loop is shown in Figure 1.2. The system includes the actuator and driver, position error signal (PES) demodulator, timing generation and position control subsystems. In an embedded servo, the servo information are pre-written equally spaced sectors on the disk. From the demodulated signal, the data is digitized and sent into a digital signal processor (DSP) for implementation of the control law. The control law typically implements a discrete-time, state-space regulator for track following (when the head is stationary over a single track) and a reference-trajectory-following state-space controller for track seeking (moving the head from one track to another). The control law is designed to minimize the effects of internal and external disturbances on the PES. The internal disturbances are caused by spindle motion, the airflow over the disk and arms, the noise in sensing the PES, and reactions from track seeking. The external disturbances are mostly due to shock and vibration. The output of the controller is converted back to an analog signal and sent to a power amplifier, which converts the desired voltage into current source, driving the actuator to set the position of read/write heads.

The average seek time, which is defined as the time to move across 1/3 of the recorded data band and settle on a given track, is typically less than 5 ms in a high performance HDD. The nature of the seeking servo is to force the actuator angular velocity to follow an ideal angular velocity profile that will guarantee the shortest possible seek time with minimum jerk such that the recording head arrives at the desired track at a very small angular velocity. The actuator's angular velocity is digitally estimated by an algorithm in the microprocessor that uses position error information obtained from each servo sector during the seek process. The seek mode is usually implemented as a proportional-derivative type of control with a constant monitoring of the remaining distance to the target track. This must be done in a smooth manner so as to minimize any unnecessary excitation of mechanical resonances in the disk drive which will cause a mechanical ringing problem during the track follow portion of the servo operation.

When the actuator is less than one track pitch away from the target track, the settle mode takes over from the seek mode. At this point, the settling control should guide the center of the recording head to be within a certain position error tolerance of the target track center line for a faster track following switching. This stage becomes more and more important and widely studied since the settling mode is one of the major contributors of TMR.

In the track following mode, the servo objective is to stay as close to the track center line as possible for reading and writing information. The main difficulty in the mode is caused by the various position error sources existing in the servo channel. The track misregistration (TMR) is used to measure the offset between the actual head position and the track center [100]. The TMR is defined as three times standard deviation of PES and is approximately 12% of the track to track pitch in normal operation. The goal of servo control system is to minimize the TMR in the presence of measurement and process noise and disturbance.

The servo must operate with the following factors: (1) finite control authority; (2) position reference noise; (3) uncertain high-frequency actuator dynamics; (4) sensor noise and sensor nonlinearities; (5) no absolute position reference during most operations; (6) nonzero saturation recovery time in the power amplifier; (7) variable actuator parameters. In short, the disk-drive represents a typical mass produced high performance servomechanism.

1.2.2 Challenges of Servo Control

Due to these trends, hard disk drive technology also faces many challenges. Two challenges of servo control which are most relevant to this thesis are discussed in this section.

1) Sample rates

The multiplexing of position information with user data on hard disks creates a set of competing objectives. On one hand, larger areal density to some extent means increased track density which demands increased position accuracy and finally requires higher control bandwidth. On the other hand, larger areal density means increasing user data capacity, in other words, reducing servo information which results in limited sampling frequency in our servo system. These tradeoffs have limited the achievable sample rates to the range of 6-30 kHz. This in turn has limited the achievable tracking closed-loop bandwidth to the range of 500-3000 Hz.

This has led to a fair amount of work in multirate servos, where the control output is changed at a higher frequency than the sample rate of the PES. Rick Ehrlich had been pursuing the idea of multirate control ever since he was at Hewlett-Packard. Carl Taussig continued this work, coming up with unpublished results quite similar to those reported by W.W. Chiang (out of IBM San Jose) [33]. It turns out that Rick Ehrlich had continued his multirate work at Quantum and was getting similar results. Their finding show that if the PES sample rate was relatively low, say, less than eight times the open-loop crossover, keeping everything else constant and raising the output sample rate by a factor of three or four over the input sample rate could result in a closed-loop bandwidth improvement of roughly 20%. If, on the other hand, the PES sample rate was already at roughly 20 times the open-loop crossover, then the improvement was far smaller. The improvement of bandwidth is due to the use of multirate control in a low PES sampling frequency system. We note that there are control systems that were designed to have high sampling frequencies compared with the system closed-loop bandwidth, and in such system the improvement due to using the multirate control may not be so significant.

Multirate on the main loop has found applicability in the use of multirate notches. The ability to design sharp notch filters had been limited by the relatively low sample rate of PES compared to the frequency of the actuator resonances. To combat this, a group of engineers at Quantum (Rick Ehrlich, David Jeppson, and Phil Weaver) came up with a multirate notch filter [87]. A similar approach was used by Don Fasen at HPś Disk Memory Division, although this was never published or patented. The multirate approach has also been applied to the use of auxiliary sensors in disk drives. In cases where the sensor can sample information independently of the structure of the position information on the disk, performance can be improved by raising the sample rate of the auxiliary sensor and the update rate of the control law [2] [15]. These auxiliary sensors come in three main forms: accelerometers for rejection of internal and external disturbances, extra sensing of the back EMF mentioned above, and instrumented suspension.

Fujimoto et. al proposed to use multirate discretization and its inverse together with a disturbance observer to design feedforward controller which makes the disturbance effect become zero at every inter sample point [42]. Initial value compensator configuration was used to improve the performance of their proposed controller. We found the scheme of multirate discretization and its inverse can be used to improve the performance of periodic disturbance cancellation method which will be discussed later.

2) Disturbance rejection

Another challenge in HDD servo is disturbance rejection. With increasing track density in HDD in recent years, it has been identified that runout is one of the main contributors to track misregistration (TMR). Repeatable runout (RRO) is caused by non-repeatable runout (NRRO) in the servo writing and disk wrapping process, disk slip caused by thermal expansion of the disk etc [89]. The internal model principle (IMP) [38] states that a model of the disturbance generation system must be included in the feedback system for disturbance rejection. According to

IMP, only RRO and NRRO within the servo bandwidth can be attenuated. A special controller, runout compensator, is necessary for compensation of those close to or beyond the servo bandwidth. Basically, the RRO is a repeatable periodic signal and is phase locked to the spindle rotation [89]. It can be considered as a periodic disturbance with fixed frequency as long as the rotation speed is fixed. However, we cannot deal with disturbance with fixed frequency only. As the rapid growth of mobile device and consumer electronic products, disk drives for mobile applications are at a critical point since high capacity is needed but it must prove its robustness and overall reliability to the mobile marketplace. As for mobile devices, for example, the rotation speed of a mobile drive, the paces of a running man with a storage device may change due to the mobile feature, disturbance to the mobile storage product on an automobile may have various frequency due to the shock status and engine speed change etc. All these situations demand a more robust compensation scheme which is not only effective to disturbance signal with fixed frequency but also effective to disturbance with changing frequencies.

One of the concepts to become popular in disk drive control systems at the end of the 1980s was the use of repetitive control to cancel the effects of the spindle eccentricity. Some early unpublished work had been done by Mike Sidman for the DEC RC25 in 1978. However broad use in the drive industry started when Masayoshi Tomizuka's group was working on practical applications of repetitive control as a solution to repetitive disturbances in rotating machinery. Since the drive DSPs code was not accessible, they used the notion of an add-on controller that would augment the nominal loop to remove the harmonic disturbances [67] [31]. These studies also included adaptive feedforward harmonic cancellers, which were shown to have some equivalence with repetitive controllers.

Most previously published work in the area of HDD disturbance rejection has dealt with cancellation of synchronous disturbance [83]. While there are significant similarities between the problems of rejection synchronous and nonsynchronous disturbances, the amplitude and phase of the synchronous disturbances typically change very slowly with time, allowing very low adaptation gains, with correspondingly small effects on the characteristics of the overall servo loop. Because many nonsynchronous disturbances are driven by white noise processes or machine vibration etc., their more rapidly changing magnitude and phase require relatively high adaptation gains which can significantly affect the stability and transient response of the overall servo loop [36]. Solutions to this kind of narrow-band disturbances are studied in recent years, including internal model method [36] and peak filter method in Dual-Stage HDD [93]. These methods do a very good job of rejecting narrow-band disturbances because of the high peak in the open-loop gain at the expected frequency of the disturbance. As a result, the transient response becomes sluggish because of the same peak. Thus a controller designed to deal with both steady-state and transient conditions is needed to solve this problem.

1.3 Motivation of the Thesis

H. S. Lee in his keynote speech at Asia-Pacific Magnetic Recording Conference 2004 predicted that the Compound Annual Growth Rate (CAGR) of the consumer electronic (CE) products is 28%. The new CE products are composed of digital appliances and mobile storage. As such, a more robust compensation scheme is needed which is not only effective to disturbance signal with fixed frequency but also effective to disturbance with changing frequency.

Many repetitive algorithms have been studied to cope with this problem. Adaptive Feedforward Cancellation (AFC) Scheme has been proved to be a very effective one. However, 1) this previous work has never paid attention to the hardware restriction on the sampling scheme. To make a target of achieving higher control bandwidth with limited sampling frequency, multirate sampling control have been studied as one viable approach to relax the PES sampling frequency requirment. 2) this conventional AFC scheme already has a pre-compensator which shapes the plant to be zero phase to avoid the amplification of unconcerned disturbance frequency as well as to improve the robustness of the AFC scheme. However, the design of the pre-compensator depends on whether the plant is a minimum phase system or not and it cannot shape the plant to be zero phase over high frequency range. Therefore the unselected disturbance harmonics over this frequency range maybe amplified which is not satisfactory.

As we know now, through multirate discretization, we can attain the inverse model of a system without considering its unstable zeros . Therefore, this thesis combines the pre-compensator attained from multirate inverse and the AFC scheme to improve the performance of periodic disturbance rejection scheme in HDD servo. We also discuss the robustness of the proposed scheme against parameter variation and time varying periodic disturbance. The later case shows how effective the proposed scheme is in compensating for time-varying runout disturbances.

1.4 Thesis Organization

The rest of the thesis is organized as follows:

Chapter 2 gives an overview of the multirate digital control design and multirate discretization through multirate sampling are discussed in this chapter. Then the plant inverse through multirate discretization is discussed and the comparison between the proposed scheme and usual scheme is made.

Chapter 3 presents a periodic disturbance compensator design for HDD tracking servo system. Various kinds of repetitive algorithms which are designed to deal with periodic disturbance are introduced. Comparison between the proposed scheme and conventional scheme is made.

Chapter 4 gives the application example of applying the proposed scheme to a spin stand servo system. Simulation configuration and experiment setup are presented. Implementation issues, simulation and experiment results are given in the form of comparing with the conventional scheme.

Chapter 5 summarizes the dissertation and proposes some further topics.

Chapter 2

Multirate Control and Plant Inverse

Many applications have included the multirate sampling control. For example, in the head positioning system of hard disk drives, the head position is detected by the servo signal embedded in disks discretely. Thus, the sampling frequency is restricted because it is determined by the rotational frequency and number of the servo signals. On the other hand, the control frequency of the actuator (voice coil motor) can be set faster than the sampling frequency of the head position. Another example is the visual servo system of robot manipulators. Although the sampling period of the vision sensor such as a CCD camera is comparatively slow (over 33 ms), the control period of the joint servo is very fast (less than 1 ms). Therefore, multirate controllers have been developed and implemented in the visual servo systems. The third example is the velocity or position control of industrial motors with low precision encoders. In these systems, the sampling period cannot be set too short, because the velocity information cannot be detected due to the low resolution of the encoder. Moreover, multirate filter bank is one of the hot research topics in the field of signal processing. Recently, sampled-data control theory is applied to design of the filter banks based on the continuous-time signal [30, 98]. In recent years, high performance and high precision intelligent encoders are being developed which have signal possessors and communication equipment. If these encoders are implemented to the motion control systems, the sampling frequency is fixed to the communication speed. Thus, the multirate sampling control will play a more important role in the future practical motion control systems.

2.1 Advanced Sampled-data Control Theory

As the theory background of the multirate control theory, advance sampled-data control theory has been developed very rapidly from 1990 [28, 30]. The advantage of this theory is that the intersample behavior can be directly considered and designed.

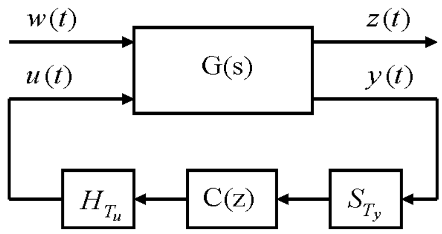

Figure 2.1: General setup of multirate sampled-data H_∞ control problem.

Fig. 2.1 shows the general setup of the multirate sampled-data H_∞ control problem, where $G(s)$ is a continuous-time generalized plant and $C(z)$ is a multirate controller. S_{T_y} and H_{T_u} denote a sampler and a hold respectively. T_y and T_u are the measurement sampling period and the control period respectively. The exogenous input $w(t)$ contains disturbances and reference signals, and the controlled output

$z(t)$ is the signal which should be made small or zero. The control input u is generated by the discrete-time controller, and the measured output $y(t)$ is an input variable of the digital controller.

The formulation of the advanced sampled-data theory is to find the digital controller $C(z)$ to minimize typically H_2 or H_∞ norm from w to z. For single-rate case, Bamieh and Pearson [13, 14], Kabamba and Hara [65], Yamamoto et al. [57] have shown the solvability conditions and computational procedures of the controller. For multi-rate case, Chen and Qui [29] provides explicit solutions for this problem taking into account the causality constraints. More recently, multi-rate H_∞ control design methodology for HDDs [77, 58] has been found successful application.

However, in the present situation, this theory has solved only H_2 and H_∞ control problems. Thus, it is not always applicable to all problems, since H_2 and H_∞ synthesis is not always effective and it makes several assumptions in obtaining the solutions. More practical improvements will be desired in the future.

2.2 General Multirate Control System

Multirate systems differ from single rate sampled data systems in that the switches do not operate at the same sampling rate [66, 68]. A block diagram of general multirate system is shown in Figure 2.2. In the figure, $r_1, r_2, \cdots, r_n$ are reference inputs, $y_1, y_2, \cdots, y_n$ are plant outputs, H_{ic}, H_{ip}, $T_{ic}, T_{ip}, (i = 1, 2, \cdots, n)$ are holders and samplers for controller and plant respectively. In a multirate system, they could be of any different value.

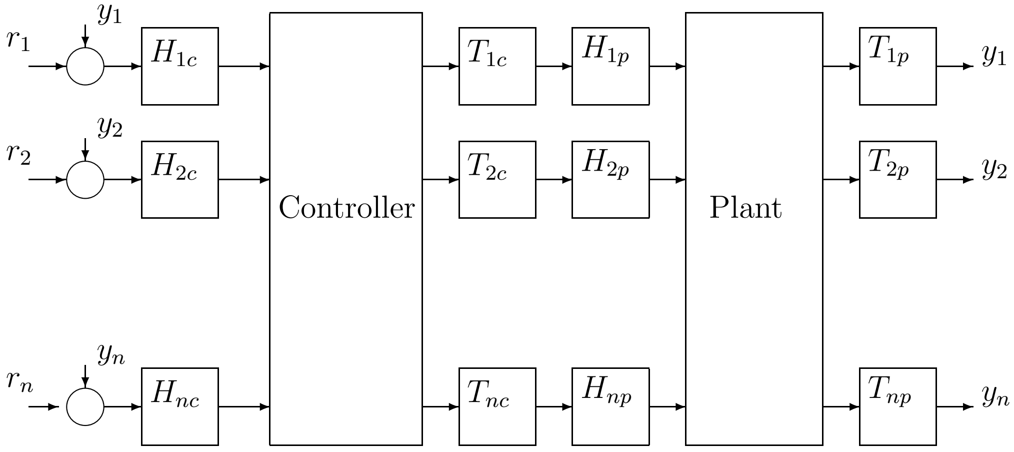

Figure 2.2: MIMO multirate system.

Multirate control techniques started in the 1950's as an analysis tool for aerospace engineering applications. In such a system, it is impossible to operate the thousands actuators of different electro-mechanical constants at the same rate. Multirate sampling provides the opportunity to allocate sampling rates, and thus real-time computing power, more efficiently. Furthermore, multirate control can reduce hardware costs in that the computation rates required of A/D and D/A converters frequently depend on their sampling rates. This methodology can be applied in a large range of industrial digital controllers.

In addition to the case where the multirate sampling is required, multirate control schemes bring about several advantages. By applying multirate control scheme, more design freedom can be provided at the cost of consuming more computation power. The use of multirate strategies can improve the time or frequency specifications of the process output, modifying the overshoot, the settling time, hidden oscillations, or the phase and magnitude margins. For example, in a classic water-level regulation loop of a boiler control system, by using the multirate controller strategy with the control updating rate of the inner loop m times faster than that of the outer-loop, disturbance rejection can be much enhanced.

As the foundation, Kalman and Bertram [66] gave the first substantial treatment of multirate systems from the state space perspective. They presented a method for forming a discrete-time state model of a multirate sampled-data plant. For a linear and time invariant plant and the general case of multirate sampling, the discrete time model is time varying. For the special case where all sampling rate ratios are rational numbers, the discrete time model is periodically time varying with the same period as the sampling schedule.

Granc [68] also analyzed works for multirate systems in the frequency domain by proposing a switch decomposition method. The idea was to attach a phantom sampler to the input or output port of a single-input, single-output (SISO) system and operate it at some integer multiple of the basic sampling rate to detect intersample ripple. Based on this method, Sklansky [84] further developed the frequency decomposition method to determine the transfer function for the multirate system.

In principle, the frequency decomposition and switch decomposition methods can be used to determine transfer functions of many multirate systems of practical interest. In practice, however, those methods are extremely cumbersome. Ragazzini and Franklin [39] described an application of the switch decomposition method to a SISO system having two samplers with sampling periods T_s and $\frac{T_s}{r}$. They pointed out that the resulting transfer function has r forward paths, each with delay and advance operators.

Glasson et al. reviewed the general methods used in dealing with multirate system analysis in their recent paper [45]. They developed a closed-loop model of general multirate digital control systems. The model completely represents system behavior at a base sampling rate and at the integral multiple sampling rates in the system.

M. Araki and K. Yamamoto generalized a certain kind of multirate system, presented its state-space description, transfer characteristics and Nyquist criterion. By introducing the concepts of “multirate impulse modulation” (MIM) and“symmetric-coordinate multirate impulse modulation” (SMIM), four stability criteria are derived.

Fujimoto et al. proposed a perfect tracking control methode based on multirate feedforward control [41], which eliminates the unstable zero problem and is independent of the feedback characteristics. Furthermore, the states of the plant match the desired trajectories at every sampling point of reference input.

Most mathematical analyses convert the original multirate system to an equivalent single rate system, either at the slowest common base rate or at the fastest common rate. The obvious disadvantage of the first method is that such a scheme will definitely lose most of the useful information between the gaps of faster sampling instances. The second method, on the other hand, could retain such system information, although the overall dimension of the augmented system will increase. Generally such a system is a high dimension MIMO system.

In addition to the various descriptions of the multirate sampled data system, multirate control system properties have also been intensively researched. Generally, with the assumption of proper sample and hold rates, the stability and observability will still be preserved if the original multirate system is stabilizable and detectable. The separation principle still holds for the design of a multirate controller for the original system, *i.e.*, we can design the regulator and estimator for the control system respectively.

There are five well-recognized methods of design and synthesis [16]:

(1) successive loop closures (SLC),

(2) pole placement,

(3) the singular perturbation method,

(4) the Linear Quadratic Gaussian (LQG) method,

(5) parameter optimization methods.

The successive loop closure method is an indirect approach to multirate synthesis in that a multirate compensator is synthesized by successively closing a series of single rate control loops. This method was mainly adopted in the early days of multirate systems. The advantages of the SLC method are: 1) only conventional (typically SISO) single rate synthesis techniques are required; 2) the resulting compensators usually have a simple and low order structure. The disadvantages of the SLC method is that it is an ad hoc method for dealing with the cross coupling between control loops because the nth loop can only be designed to respond to the cross-coupled effects of the $(n+1)th$ loop as disturbances.

Pole placement method is widely used in today's controller design in that it is simple and straight forward to design the system according to the specific criterion they wish to obtained in time or frequency domain. Many analysis results have been given in the research papers. However, since it is more often a trial and error method than a direct optimal one, it is not always guaranteed to achieve an optimal control design. Furthermore, in a multirate system, some hidden issues such as the intersample behaviors may not be dealt with via pole placement.

The singular perturbation method was first developed as an analysis tool firstly for continuous time systems, taking advantage of the multiple time scale dynamics that often occur in control systems. It would seem that an extension to multirate sampled data control systems should follow naturally, given that the principal motivation for multirate sampling has always been to take advantage of those same multiple time scales.

The advantage of the LQG method for multirate control law synthesis is that the control laws for all control loops are synthesized simultaneously, taking into account all dynamic coupling between control loops. The disadvantages are the same as those for the LQG method for continuous time control law synthesis: practical performance and stability robustness objectives are usually difficult to achieve via the minimization of a quadratic performance index. In short, LQG multirate control laws can provide useful benchmarks for performance comparisons, but they may not necessarily be good for practical applications.

Parameter optimization methods for multirate control law synthesis combine the advantages of the LQG and the successive loop closures synthesis methods. Like the LQG method, parameter optimization methods simultaneously account for all dynamic coupling between control loops. Like the SLC methods, parameter optimization methods allow the synthesis of multirate control laws of arbitrary structure and dynamic order. The typical parameter optimization method requires that the control law structure and its parameters to be optimized be prescribed. A numerical search is used to optimize those parameters such that a quadratic performance index is minimized possibly subject to constraints on those parameters. Although it inevitably requires a numerical search, the best system performance can be expected [9, 16, 25].

Next, we will discuss multirate sampling and plant inverse via multirate discretization.

2.3 Multirate Sampling and Plant Discretization

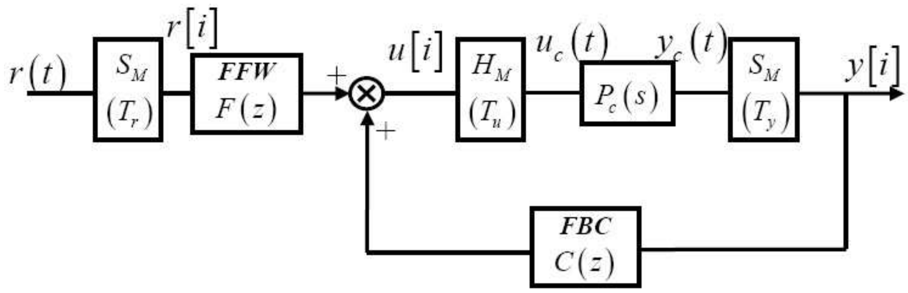

Figure 2.3: Two-degree-of-freedom digital control system.

Fig. 2.3 shows the block diagram of a typical two-degree-of-freedom digital control system with the plant $P_c(s)$ being the actuator, $C(z)$ and $F(z)$ being the feedback controller and feedforward controller respectively. A digital tracking control system usually has two samplers for the reference signal $r(t)$ and the output $y(t)$, and one holder on the input $u(t)$, as shown in Fig. 2.3. Therefore, there exist three time periods T_r, T_y, and T_u which represent the periods of $r(t)$, $y(t)$, and $u(t)$, respectively. In the conventional digital control systems, these three periods are made equal to the longer of the two periods T_u and T_y. If there is not only one sampling period in the system, i.e. T_r, T_y, and T_u are not the same, the system can be considered as a multirate system.

In the servo systems of HDDs, the head position is detected by the discrete servo signals embedded in the disks and in order to maximize data capacity, these servo signals are limited. Thus, the output sampling period T_y which is decided by the number of these signals and the rotational frequency of the spindle motor is also limited. T_y is also determined by the speeds of the sensor and the A/D converter. The input period T_u is generally decided by the speeds of the actuator, the D/A converter or the calculation on the CPU. Thus, the conventional digital control systems make these three periods equal to the longer period between T_u and T_y. The longer period is defined as the frame period T_f and the z-operator is defined as $z \triangleq \mathrm{e}^{sT_f}$. In our case, the sampling periods of plant output should be long [42][43]. Thus, we focus on the case $T_f = T_r = NT_y = NT_u$. Although T_u is decided in advance by the hardware restrictions, the plant output can be detected at the same period, i.e. $T_u = T_y$. The frame period is set to $T_f = T_r$, as shown in Fig. 2.4.

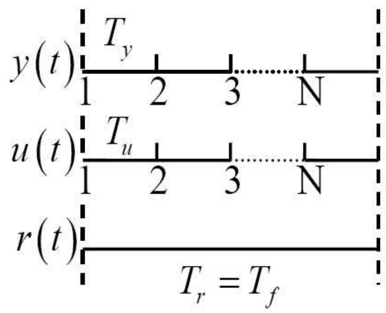

Figure 2.4: Multirate sampling $T_f = T_r = NT_y = NT_u$.

Consider the continuous-time nth-order single input single output (SISO) plant $P_c(s)$ described by

$$\dot{x}(t) = A_c x(t) + B_c u(t), \tag{2.1}$$

$$y(t) = C_c x(t) + D_c u(t). \tag{2.2}$$

The discrete-time plant $P[Z_s]$ discretized by single rate sampling period T_y $(= T_u)$ becomes

$$x[k+1] = A_s x[k] + B_s u[k], \tag{2.3}$$

$$y[k] = C_s x[k] + D_s u[k], \tag{2.4}$$

where $x[k] = x(kT_y)$, $z_s \triangleq e^{sT_y}$ and $A_s = \mathrm{e}^{A_c \frac{T_f}{N}}, B_s = \int_0^{T_f/N} \mathrm{e}^{A_c \tau} B_c \mathrm{d}\tau$.

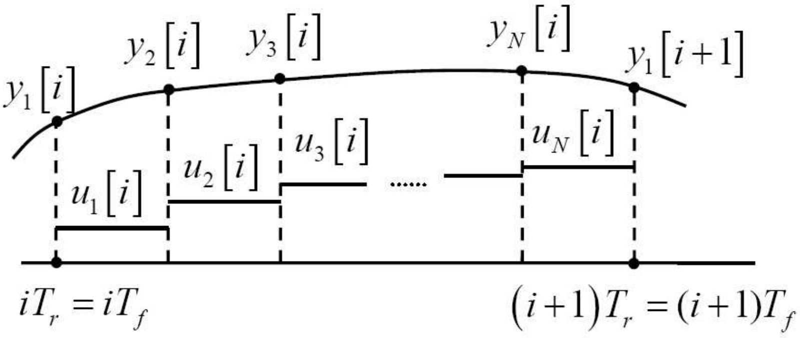

Figure 2.5: Intersample of multirate sampling.

The discrete-time plant $P[z]$ discretized by generalized multirate sampling control as shown in Fig. 2.5 can be represented by

$$x[i+1] = Ax[i] + Bu[i], \tag{2.5}$$

$$y[i] = Cx[i] + Du[i]. \tag{2.6}$$

where $x[i] = x(iT_f)$, $z \triangleq e^{sT_f}$, and the multirate input and output vectors u and y are defined as,

$$u[i] \triangleq [u_1[i], \cdots, u_N[i]]^T = [u(kT_y), u((k+1)T_y), \cdots, u((k+N-1)T_y)]^T \tag{2.7}$$

$$y[i] \triangleq [y_1[i], \cdots, y_N[i]]^T = [y(kT_y), y((k+1)T_y), \cdots, y((k+N-1)T_y)]^T \tag{2.8}$$

and matrices A, B, C, D can be calculated by

$$\left[\begin{array}{c|c} A & B \\ \hline C & D \end{array}\right] \triangleq \left[\begin{array}{c|cccc} A_s^N & A_s^{N-1}B_s & A_s^{N-2}B_s & \cdots & B_s \\ \hline C_s & D_s & 0 & \cdots & 0 \\ C_sA_s & C_sB_s & D_s & \cdots & 0 \\ \vdots & \vdots & \vdots & \cdots & \vdots \\ C_sA_s^{N-1} & C_sA_s^{N-2}B_s & C_sA_s^{N-3}B_s & \cdots & D_s \end{array}\right] \tag{2.9}$$

where $P[z_s] = A_s, B_s, C_s, D_s$ is the plant discretized by the zero order hold on $T_y(= T_u)$ and $z_s \triangleq \mathrm{e}^{sT_y}$, $A_s = \mathrm{e}^{A_c \frac{T_f}{N}}, B_s = \int_0^{T_f/N} \mathrm{e}^{A_c\tau} B_c \mathrm{d}\tau$. It becomes a n-dimensional plant with N inputs and N outputs. It is very easy to verify,

$$x[k+1] = A_s x[k] + B_s u[k],$$

$$x[k+2] = A_s x[k+1] + B_s u[k+1] = A_s^2 x[k] + A_s B_s u[k] + B_s u[k+1],$$

$$x[k+3] = A_s x[k+2] + B_s u[k+2] = A_s^3 x[k] + A_s^2 B_s u[k] + A_s B_s u[k+1] + B_s u[k+2],$$

$$\cdots$$

$$x[k+N] = A_s^N x[k] + A_s^{N-1} B_s u[k] + \cdots + A_s B_s u[k+N-2] + B_s u[k+N-1],$$

$$y[k] = C_s x[k] + D_s u[k],$$

$$y[k+1] = C_s x[k+1] + D_s u[k+1] = C_s A_s x[k] + C_s B_s u[k] + D_s u[k+1],$$

$$y[k+2] = C_s x[k+2] + D_s u[k+2] = C_s A_s^2 x[k] + C_s A_s B_s u[k] + C_s B_s u[k+1] + D_s u[k+2],$$

$$\cdots$$

$$y[k+N-1] = C_s A_s^{N-1} x[k] + C_s A_s^{N-2} B_s u[k] + \cdots + C_s B_s u[k+N-2] + D_s u[k+N-1],$$

$$\left[\begin{array}{c} x[k+N] \\ \hline y[k] \\ y[k+1] \\ \cdots \\ y[k+N-1] \end{array}\right] = \left[\begin{array}{c|cccc} A_s^N & A_s^{N-1}B_s & A_s^{N-2}B_s & \cdots & B_s \\ \hline C_s & D_s & 0 & \cdots & 0 \\ C_sA_s & C_sB_s & D_s & \cdots & 0 \\ \vdots & \vdots & \vdots & \cdots & \vdots \\ C_sA_s^{N-1} & C_sA_s^{N-2}B_s & C_sA_s^{N-3}B_s & \cdots & D_s \end{array}\right].$$

2.4 Plant Inverse

2.4.1 Plant Inverse Based on Pole/Zero and Phase Cancellation

If the equivalent plant $O(z)$ is not a zero phase system, pole/zero cancellation and phase cancellation can be used to design $\tilde{O}^{-1}(z)$ to shape the plant such that $O(z)\tilde{O}^{-1}(z)$ is close to a zero-phase system [88]. Without loss of generality, suppose that the equivalent plant $O(z)$ can be expressed as

$$O(z) = \frac{N(z)}{D(z)} = \frac{b_0 z^m + b_1 z^{m-1} + \cdots + b_m}{z^n + a_1 z^{n-1} + \cdots + a_n}. \tag{2.10}$$

Because the equivalent plant is the closed-loop system under nominal controller for our case, all the roots of $D(z)$ are inside the unit circle in the Z-plane, and the roots of $N(z)$ can be either inside, on or outside the unit circle.

If the equivalent plant $O(z)$ is a minimum phase system, i.e. all the roots of $N(z)$ are inside the unit circle, thus all the poles and zeros of the plant are cancellable. Therefor $P(z)$ can be designed as

$$\tilde{O}^{-1}(z) = \frac{D(z)}{z^d N(z)}, \tag{2.11}$$

where $d = n - m$. After that all the poles and zeros of $O(z)$ are cancelled by $\tilde{O}^{-1}(z)$.

If the plant is a non-minimum phase system, and suppose that there is no zeros on the unit circle, then the numerator polynomial $N(z)$ can be factored into two parts such that,

$$N(z) = N^s(z)N^u(z), \tag{2.12}$$

where $N^s(z)$ includes stable zeros which are cancellable, and $N^u(z)$ includes zeros which are not inside the unit circle. Then $\tilde{O}^{-1}(z)$ can be designed as

$$\tilde{O}^{-1}(z) = \frac{D(z)N^{u^*}(z)}{z^{d+2u}N^s(z)}, \tag{2.13}$$

where u is the order of $N^{u^*}(z)$. $N^{u^*}(z)$ can be designed according to Butterworth transforms. If $N^u(z)$ is represented as,

$$N^u(z) = d_0 + d_1 z + \cdots + d_u z^u, \tag{2.14}$$

then $N^{u^*}(z)$ can be designed as,

$$N^{u^*}(z) = d_u + d_{u-1} z + \cdots + d_0 z^u. \tag{2.15}$$

Note that $\frac{N^{u^*}(z)}{z^u}$ is the complex conjugate of $N^u(z)$ when $z = \mathrm{e}^{j\omega T_s}$. Therefore, $N^u(z)\frac{N^{u^*}(z)}{z^u}$ is positive real.

2.4.2 Plant Inverse via Multirate Discretization

Using multirate discretization, the system becomes an n-dimensional plant with N inputs and N outputs, with D being a square matrix of full rank depicted by equation (2.9). Thus we can get its inverse state-space model $\tilde{O}^{-1}(z) = \{A, B, C, D\}^{-1}$ directly:

$$\left[\begin{array}{c|c} A & B \\ \hline C & D \end{array}\right]^{-1} \triangleq \left[\begin{array}{c|c} A - BD^{-1}C & BD^{-1} \\ \hline -D^{-1}C & D^{-1} \end{array}\right] \tag{2.16}$$

2.4.3 Example

Let us use a simple example to illustrate the advantage of the multirate inverse scheme.

Given a first order single input single output system described by transfer function as,

$$O(s) = \frac{s-10}{s+23}. \tag{2.17}$$

Its single rate discrete form with sampling frequency ($1/T_r = 1/T_u = 1/T_y = 15$ kHz) by ZOH method becomes,

$$O_1(z) = \frac{0.9989z - 0.9996}{z - 0.9985}. \tag{2.18}$$

After discretized by dual rate sampling (i.e. $1/T_r = 1/(2 \times T_u) = 1/(2 \times T_y) = 15$ kHz), using equation (2.9), its state space representation is,

$$O_2(z) = \left[\begin{array}{c|c} A & B \\ \hline C & D \end{array}\right] = \left[\begin{array}{c|cc} 0.9985 & 0.0002664 & 0.0002666 \\ \hline -4.125 & 1 & 0 \\ -4.122 & -0.0011 & 1 \end{array}\right]. \tag{2.19}$$

While there's one unstable zero of the plant, using the pole/zero and phase cancellation scheme, i.e. the pseudo inverse obtained using equation (2.13) is,

$$\tilde{O}_1^{-1}(z) = \frac{(z-0.9985)(0.9989-0.9996z)}{z^2} \tag{2.20}$$

the phase of the shaped plant $O(z)\tilde{O}^{-1}(z)$ is the same as $\frac{1}{z}$.

The dual rate inverse model of 2.19) using equation (2.16) is thus,

$$\tilde{O}_2^{-1}(z) = \left[\begin{array}{c|c} A & B \\ \hline C & D \end{array}\right]^{-1} = \left[\begin{array}{c|cc} 1.001 & 0.0002667 & 0.0002666 \\ \hline 4.125 & 1 & 0 \\ -4.126 & 0.0011 & 1 \end{array}\right]. \tag{2.21}$$

Fig. 2.6 shows the phase of the shaped plant $O(z)\tilde{O}_i^{-1}(z)(i = 1, 2)$ when using the two inverse scheme. When using the usual inverse scheme, the phase drops down exponentially when the frequency increases. When using multirate inverse scheme, zero phase is assured over the whole frequency range.

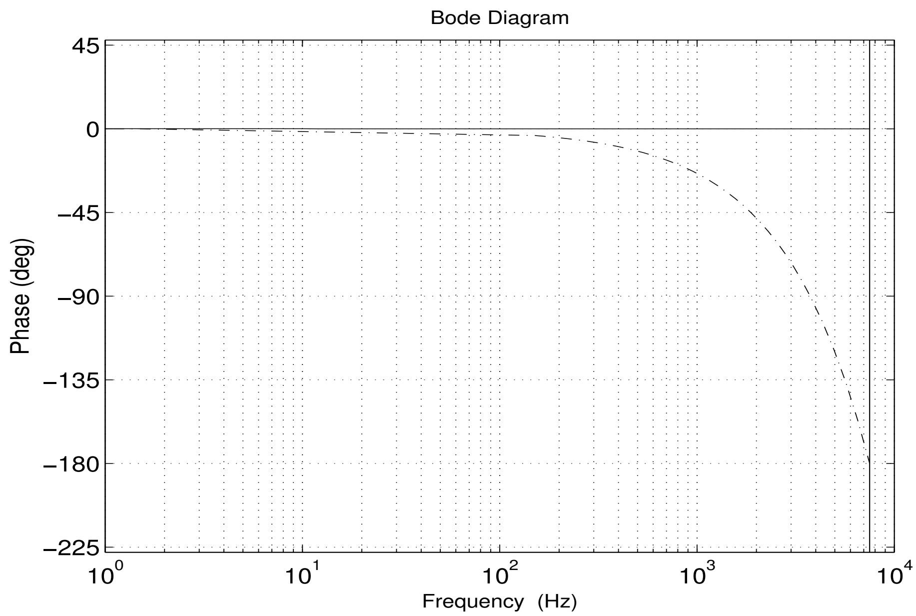

Figure 2.6: Phase of $O(z)\tilde{O}_i^{-1}(z)$. Solid line: pseudo inverse scheme $\tilde{O}_1(z)$ as equation (2.20); dash-dot line: dual rate inverse scheme $\tilde{O}_2^{-1}(z)$ as equation (2.21); plant: $O(z)$ as equation (2.18).

Chapter 3

Periodic Disturbance Compensation

Periodic disturbances is a problem which appears in a variety of applications including optical and magnetic disk drives, rotating mechanical systems and active noise control, etc. In this chapter, both conventional and the proposed schemes using multirate plant inverse for periodic disturbance compensation are discussed.

3.1 Periodic Disturbance in HDD

With increasing track density in HDD in recent years, it has been identified that runout is one of the main contributors to track misregistration (TMR). Runout consists of both a non-repeatable runout (NRRO) and a repeatable runout (RRO) component. Repeatable runout is phase locked to the spinlde rotation, and thus is a periodic disturbance. Non-repeatable runout is defined as the part of the disk runout that is not repeatable with each revolution and is 0.01 to 0.001 times smaller than the repeatable runout. NRRO with their energy in a narrow frequency band, such as disk vibration, structural vibration, external disturbances, are not periodic as their phases are not locked to the spindle speed. However, if the AFC adapts faster than the disturbance phase and amplitude variation, then RRO compensators can be used for NRRO compensations. This is one of the challenges that we are trying to solve on Chapter 3 Section 3.3. Repeatable runout (RRO) is caused by non-repeatable runout (NRRO) in the servo writing and disk wrapping process, disk slip caused by thermal expansion of the disk or HDD assembly process etc [89]. According to internal model principle, only RRO and NRRO within the servo bandwidth can be attenuated. A special controller, runout compensator, is necessary for compensation of those close to or beyond the servo bandwidth. Basically, the RRO is a repeatable periodic signal and is phase locked to the spindle rotation [89]. It can beconsidered as a periodic disturbance with fixed frequency as long as the rotation speed is fixed. The schematic diagram of disk runout is shown in Fig. 3.1.

However, as mentioned in Section 1.2.2, we cannot deal with disturbance with fixed frequency only. As the rapid growth of mobile device and consumer electronic products, disk drives for mobile applications are becoming more important since high capacity is needed but it must prove its robustness and overall reliability to the mobile marketplace. For mobile devices, for example, the rotation speed of a mobile drive, the paces of the user that carrying the device may change; disturbance to a mobile storage device on an automobile may have various frequency due to the shock status and engine speed change etc. All these situations demand a more robust compensation scheme which is not only effective to disturbance signal with

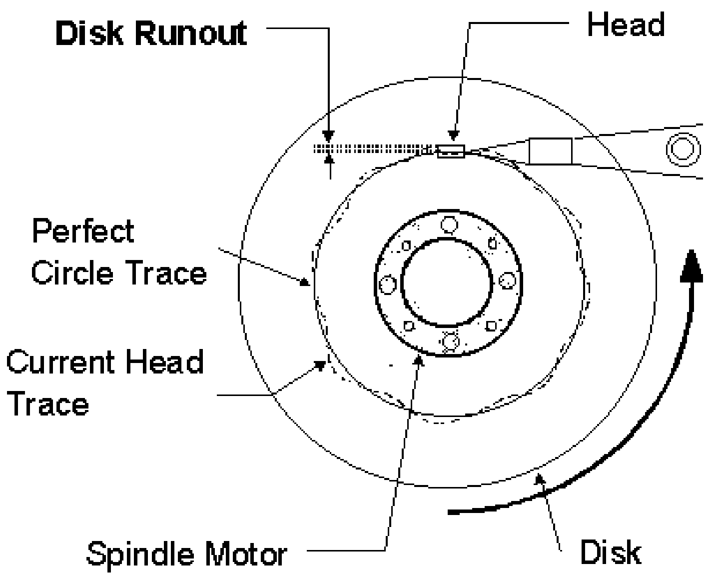

Figure 3.1: A schematic diagram of disk runout.

fixed frequency but also effective to disturbance with changing frequency.

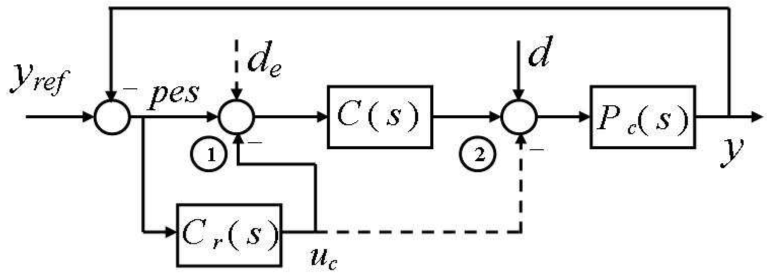

Figure 3.2: A block diagram of HDD servo with disturbance [101].

Consider a HDD servo system described in Fig. 3.2. $P_c(s)$ and $C(s)$ are plant and nominal controller respectively and $C(s)$ is assumed to be an appropriate stabilizing controller, $C_r(s)$ is the periodic disturbance compensator. d is the disturbance which may have periodic components, y_{ref} is the reference signal, u_c is the feedforward control input, y is the output and pes is the tracking error. With u_c being injected in point 1 (solid line), the system can be presented as,

$$[(Y_{ref}(s) - Y(s) - U_c(s))C(s) + D(s)]\, P_c(s) = Y(s). \tag{3.1}$$

Define tracking error $E(s)$ as,

$$E(s) = Y_{ref}(s) - Y(s). \tag{3.2}$$

With equation (3.1) and (3.2), we have,

$$E(s) = \frac{P_c(s)C(s)}{1 + P_c(s)C(s)} \left[U_c(s) - \frac{D(s)}{C(s)} + \frac{Y_{ref}(s)}{P_c(s)C(s)} \right] \tag{3.3}$$

The closed-loop transfer function from y_{ref} to y without $C_r(s)$ is,

$$O(s) = \frac{P_c(s)C(s)}{1 + P_c(s)C(s)}, \tag{3.4}$$

and we define the equivalent disturbance as,

$$D_e(s) = \frac{D(s)}{C(s)} - \frac{Y_{ref}}{P_c(s)C(s)}. \tag{3.5}$$

We can find the equivalent disturbance d_e has periodic components when y_{ref} or d is a periodic signal. And in a HDD tracking servo system, y_{ref} usually equals to zero. With equation (3.4) and (3.5), the equation (3.3) can be written as,

$$E(s) = O(s)[U_c(s) - D_e(s)]. \tag{3.6}$$

The design objective is to find $C_r(s)$ and hence $U_c(s)$ which assures the asymptotic stability of the overall system and asymptotic zero-error tracking: i.e.

$$\lim_{t \to \infty} e(t) = 0. \tag{3.7}$$

under periodic disturbance.

With $C_r(s)$, the closed-loop transfer function from y_{ref} to y is,

$$C_{L1}(s) = \frac{P_c(s)C(s)(1 - C_r(s))}{1 + P_c(s)C(s)(1 - C_r(s))}. \tag{3.8}$$

We do have an option of injecting u_c from point 2 (dashed line), the closed-loop transfer function from y_{ref} to y is,

$$C_{L2}(s) = \frac{P_c(s)(C(s) - C_r(s))}{1 + P_c(s)(C(s) - C_r(s))}. \tag{3.9}$$

We can see from equation (3.8) that if $C_r(s) \ll 1$, the feedforward compensator has little effect on the nominal servo system, and the effect depends on the $C_r(s)$ only. Similarly, from equation (3.9), if $C_r(s)/C(s) \ll 1$, the feedforward compensator has little effect on the original servo system, but the effect depends on both $C_r(s)$ and $C(s)$. In conclusion, if the $C_r(s)$ is designed independently to $C(s)$, it is better to inject compensating signal at the input point of $C(s)$ to minimize its effect on nominal servo system.

3.2 Previous Work

Various methods have been reported to deal with the periodic disturbances, and some of them can be extended to the multi-sinusoidal disturbances cases. General description of the most common approaches such as internal model principle method, repetitive control method, and adaptive feedforward cancellation method is presented in this section.

3.2.1 Internal Model Principle (IMP)

The underlying property of IMP is that a linear feedback system has perfect disturbance rejection at some frequency if and only if the controller gain is infinite at that frequency [82].

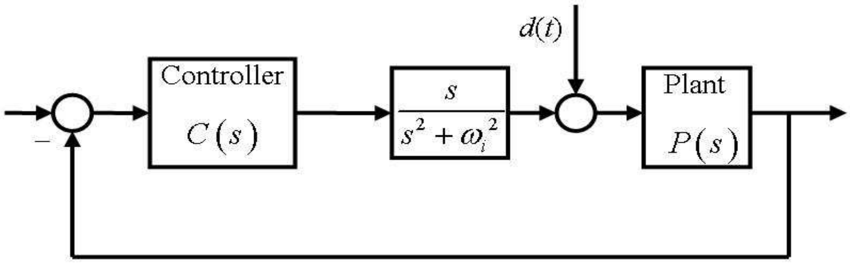

Figure 3.3: A block diagram of IMP.

Fig. 3.3 shows a controller based on the internal model principle, and a linear time-invariant (LTI) plant $P_c(s)$ is subjected to an input disturbance $d(t)$, which has the form

$$d(t) = A\sin(\omega_i t + \phi) = a_1\cos(\omega_i t) + b_1\sin(\omega_i t) \tag{3.10}$$

The compensator includes a transfer function $\frac{s}{s^2+\omega_i^2}$ to achieve perfect disturbance rejection by guaranteeing an infinite loop gain at the frequency of $d(t)$. For the asymptotic rejection of the disturbance, a proper transfer function for $C(s)$ should be chosen. That is, one has to ensure that the resulting closed loop is stable, in order to attain the desired input-output property. If the disturbance d consists of two or more sinusoids, the poles are added at all the frequencies under consideration [19].

The IMP algorithm is linear, and the convergence rate is rapid. However, when more and more poles are added on the imaginary axis, the stability problem becomes more and more difficult. Thus, the main tradeoff is between the satisfaction of closed-loop stability and the disturbance rejection, which also means that there are some performance limitations with the IMP approach.

3.2.2 Repetitive Control

Repetitive control is a subset of learning control [12]. The basic idea is to utilize the information from the previous performance of a task to improve the current performance [82]. Repetitive control has been shown to be effective for applications involving tracking of periodic reference inputs, such as trajectory control of a three link manipulator, and applications involving regulation of systems subjected to unknown disturbances of known periodicity, such as disk drive head positioning system control and eccentricity compensation in rolling.

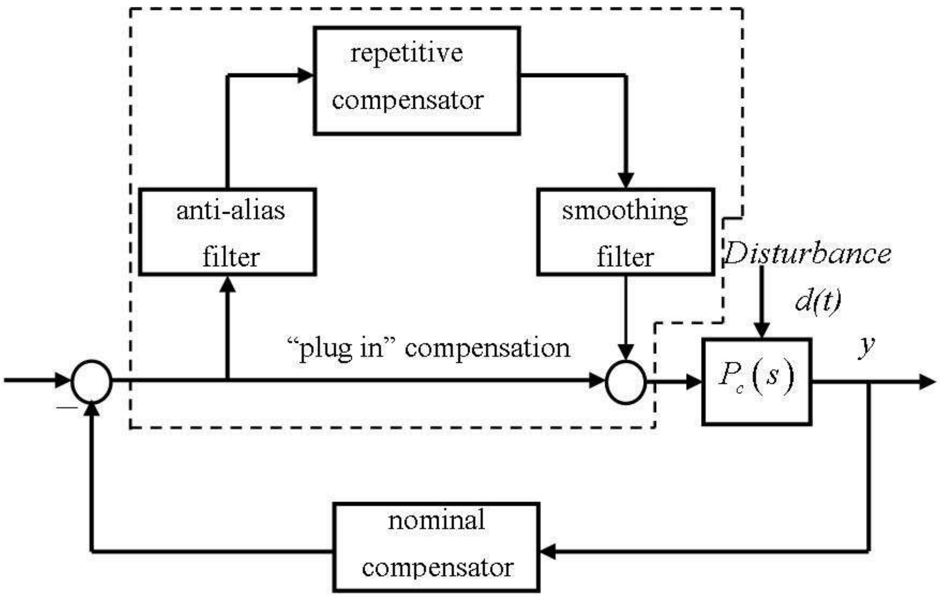

Figure 3.4: "Plug-in" repetitive compensation.

As shown in Fig. 3.4, the repetitive compensator is implemented in a "plug-in" fashion, i.e. it is used to augment an existing nominal servo. This nominal compensator is typically designed so that it stabilizes the plant and provides disturbance rejection across a broad frequency spectrum. The repetitive compensator provides specialized compensation for disturbances appearing at a known fundamental frequency and higher harmonics. Fig. 3.5 shows two examples of the "plug-in" repetitive compensator. The unit feedback of the $e^{-\tau s}$ is a generator of periodic signal which has the frequency of $2\pi/\tau$. Through tuning of the $q(s)$ and $b(s)$, the controller is able to cancel the periodic disturbance $d(t)$. Sufficient conditions for the stability issues has been discussed in [54].

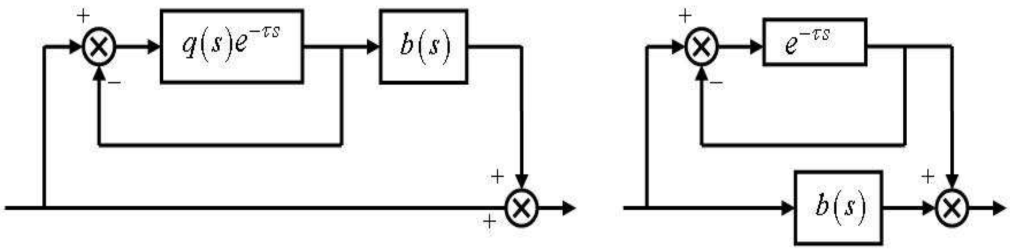

Figure 3.5: Structures of "plug-in" repetitive compensators.

Repetitive controllers can be classified into two classes: internal model based compensators and external model based compensators. The internal model based controller is a linear controller with a disturbance model, which is a simple periodic signal generator included in the repetitive compensator. It's linear and easy to analyze hence the convergence property is generally guaranteed. However, the disadvantages are that the frequency response of the original closed-loop system under the nominal controller is altered and robustness to noise and unmodelled dynamics is reduced. Both Q-filter controller and the convolution algorithm are of this type.

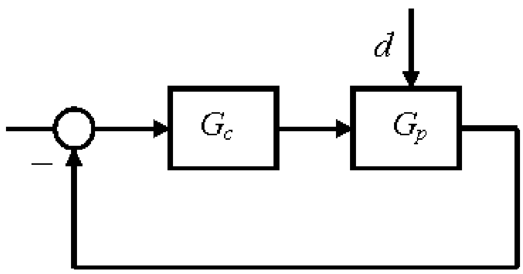

Figure 3.6: An internal model based repetitive control scheme.

Fig. 3.6 shows an internal-model-based repetitive controller, and the plant transfer function can be expressed as

$$G_p(z^{-1}) = \frac{z^{-k}B(z^{-1})}{A(z^{-1})}, \tag{3.11}$$

where k is the number of delays in the plant. The controller is of the form

$$G_c(z^{-1}) = K_r \frac{z^{-N+k}q(z^{-1})B^u(z^{-1})}{(1 - q(z^{-1})z^{-N})B^s(z^{-1})b}, \tag{3.12}$$

where K_r is the repetitive control gain, N is the number of discrete-time samples of the periodical disturbance per revolution, $B^u(z^{-1})$ is the non-minimum phase zeros (uncancellable part of the numerator), $B^s(z^{-1})$ is the minimum phase zeros (cancellable part of the numerator),

$$q(z^{-1}) = \frac{z + 2 + z^{-1}}{4}, \tag{3.13}$$

and $b = [B^u(1)]^2$. It is an inverse model of the plant, modified for unstable zeros, and the remainder of the controller places poles on the unit circle at the harmonics of the fundamental frequency. Besides, the low-pass filter $q(z^{-1})$ [31] brings the poles inside the unit circle and sacrifices high-frequency regulation, in order to improve robustness to the unmodelled dynamics and to guarantee stability [83].

The external model based compensators generate the compensation signals and inject them into the plant/controller feedback loop from outside. The external model based compensators make use of a disturbance model that can be adjusted adaptively to match the actual disturbance. Therefore the compensation scheme is much like a feedforward form and the effect of the compensators on the frequency response of the original closed-loop system can be made small. The draw back for external model based compensator is that the analysis and implementation are more complex [67].

Table 3.1: Summary of repetitive control algorithm characteristics [67]

Algorithm	Q-filter	Convolution	Basis Function	Learning
Plant Knowledge	linear model	gain and phase at disturbance frequency	linear model	linear model
Selective Frequency Rejection	no	yes	yes	no
Theoretical Complexity	low	medium	medium	high
Coding Complexity	low	medium	medium	medium
Execution Speed	fast	slow	slow	medium
Convergence Rate	fast	medium	slow	medium
Loop Gain Altered	yes	yes	no	no

3.2.3 Adaptive Feedforward Cancellation

An important class of external model based compensators is adaptive feedforward cancellation (AFC), which cancels the selective runout harmonics. In the basic AFC scheme, the Fourier coefficients of a periodic disturbance of known frequency are estimated in real-time. In a modified AFC (MAFC), the phase information of the open-loop plant transfer function is used to design a pre-compensator before the normal AFC compensator, so as to reduce the sensitivity of the adaptive controllers, as well as improve transient response. A main feature of this adaptive scheme is that there is an equivalent linear time-invariant (LTI) representation for both AFC and MAFC. This facilitates the analysis of the overall closed-loop systems very much. From the LTI representation, it is observed that both AFC and

MAFC are resonant filters, by which high gain feedback at the frequency of the runout to be cancelled is obtained.

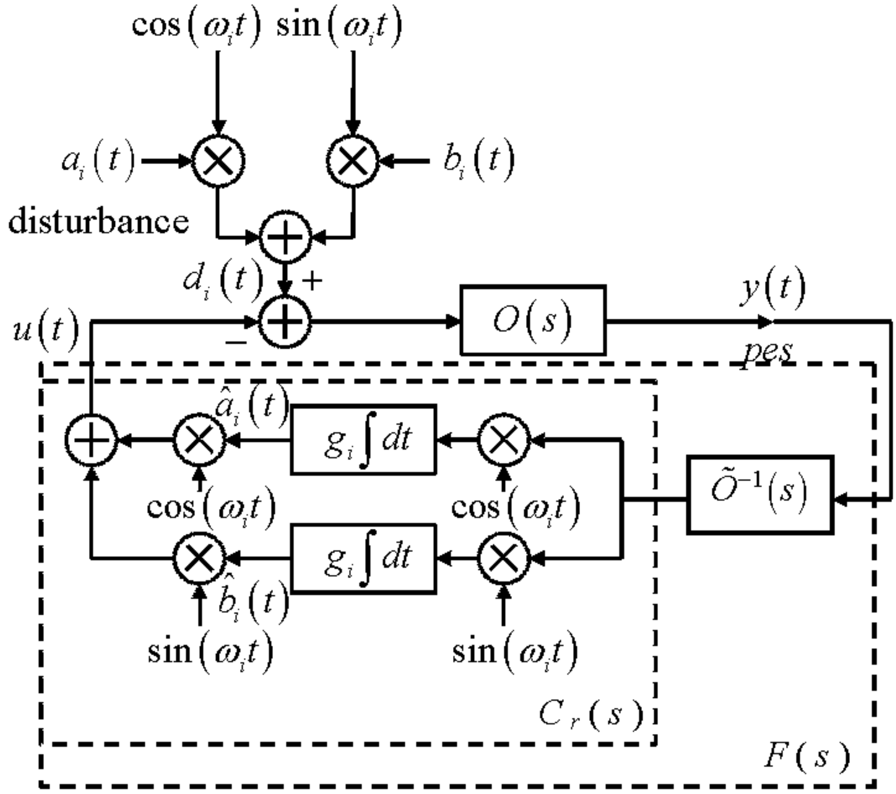

Figure 3.7: Basic AFC scheme for single frequency RRO at ω_i.

In order to design the feedforward controller $F(s)$ to cancel the RRO disturbance in the servo system, consider the equivalent periodic disturbance $d_i(\omega_i)$ shown in Fig. 3.7 represented by [89]:

$$d_i(\omega_i) = a_i \cos \omega_i t + b_i \sin \omega_i t. \tag{3.14}$$

The disturbance will be exactly cancelled when the estimates of the disturbance coefficients are such that,

$$\begin{aligned} \hat{a}_i(t) &= a_i(t), & (3.15) \\ \hat{b}_i(t) &= b_i(t), & (3.16) \end{aligned}$$

and the corrective control input $u(t)$ have the form,

$$u(t) = \sum_{i=1}^{n} (\hat{a}_i(t)\cos(\omega_i t) + \hat{b}_i(t)\sin(\omega_i t)). \tag{3.17}$$

The continuous-time adaptive low to adjust the estimates of $a_i(t)$ and $b_i(t)$ consists the following update laws as shown in Fig. 3.7,

$$\frac{d}{dt}\hat{a}_i(t) = g_i y(t)\cos(\omega_i t), \tag{3.18}$$

$$\frac{d}{dt}\hat{b}_i(t) = g_i y(t)\sin(\omega_i t), \tag{3.19}$$

with $y(t)$ being the position error signal (PES), g_i being the adaptation gain and ω_i being the desired compensation frequency. From equation (3.18), (3.19) and (3.17) and the Laplace transform characteristics we can obtain that,

$$\hat{A}_i(s) = g_i \frac{1}{2s}(E(s + j\omega_i) + E(s - j\omega_i)), \tag{3.20}$$

$$\hat{B}_i(s) = g_i \frac{j}{2s}(E(s + j\omega_i) - E(s - j\omega_i)), \tag{3.21}$$

$$U(s) = \sum_{i=1}^{n} \frac{1}{2}(\hat{A}_i(s + j\omega_i) + \hat{A}_i(s - j\omega_i)) + \frac{j}{2}(\hat{B}_i(s + j\omega_i) - \hat{B}_i(s - j\omega_i)). \tag{3.22}$$

The resulting continuous-time transfer function of $C_r(s)$ is,

$$C_r(s) = g_i \left\{ \frac{s}{s^2 + \omega_i^2} \right\}. \tag{3.23}$$

We can see $F(s) = C_r(s)\tilde{O}^{-1}(s)$ in this scheme.

The discrete-time representation of (3.18), (3.19) and (3.23) is as follows,

$$\hat{a}_i[k] = \hat{a}_i[k-1] + g_i y[k]\cos(\omega_i T_k), \tag{3.24}$$

$$\hat{b}_i[k] = \hat{b}_i[k-1] + g_i y[k]\sin(\omega_i T_k), \tag{3.25}$$

$$C_r(z) = g_i \left\{ \frac{z^2 - \cos(\omega_i T_k)z}{z^2 - 2\cos(\omega_i T_k)z + 1} \right\}, \tag{3.26}$$

where T_k is the sampling period.

Given a strictly positive real (SPR) $O(z)\tilde{O}^{-1}(z)$, the above AFC scheme is exponentially stable. When $O(z)\tilde{O}^{-1}(z)$ is not SPR, W. Messner proved that this AFC algorithm is asymptotically stable, provided $O(z)\tilde{O}^{-1}(z)$ is stable and the adaptation gain is sufficiently small [73]. The convergence rate of the AFC algorithm depends on the adaptation gains. Thus the convergence rate is limited for non-SPR systems.

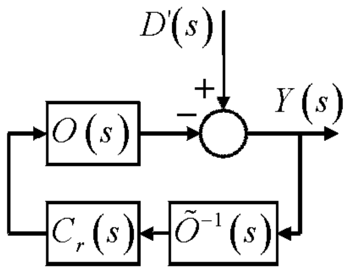

Figure 3.8: Simplified block diagram for analyzing the RRO compensation effectiveness.

Now, to analyze the effectiveness of RRO compensation using $F(s)$ for the known closed-loop servo system $O(s)$, consider an alternative equivalent RRO disturbance $D'(s)$ as shown in Fig. 3.8. The transfer function from $D'(s)$ to $Y(s)$ can be written by:

$$R(s) = \frac{1}{1 + C_r(s)\tilde{O}^{-1}(s)O(s)}. \tag{3.27}$$

When $R(e^{j\omega T}) = 1$, the loop gain at runout frequency ω equaling to 1 means there is no runout compensation. When $R(e^{j\omega T}) < 1$ or > 1, the closed-loop will attenuate or amplify the corresponding disturbance at ω.

To assure the stability of AFC algorithm as well as to avoid amplification of other RRO components, a suitable $\tilde{O}^{-1}(z)$ should satisfy: $R(z) < 1$ at other harmonics and $O(z)\tilde{O}^{-1}(z)$ must be stable. As $C_r(e^{j\omega_i T})$ is pure imaginary, the objective is to find a suitable $\tilde{O}^{-1}(z)$ that shapes the plant such that $O(z)\tilde{O}^{-1}(z)$ is close to strictly real number so that $R(\mathrm{e}^{j\omega T}) < 1$ is guaranteed.

Given the transfer function $O(z)$

$$O(z) = \frac{B^s(z)B^u(z)}{A(z)}, \tag{3.28}$$

with $B^s(z)$ and $B^u(z)$ representing stable and unstable parts respectively and u being the order of $B^u(z)$, $\tilde{O}^{-1}$ can be represented by

$$\tilde{O}^{-1}(z) = \frac{A(z)B^{u^*}(z)}{z^{d+2u}B^s(z)}, \tag{3.29}$$

where $\frac{B^{u^*}(z)}{z^u}$ is the complex conjugate of $B^u(z)$.

The phase of the shaped plant is $1/z^{d+u}$, which is near zero phase in the low frequency area and the phase will drop down exponentially when the frequency increases. Therefore the condition that $O(z)\tilde{O}^{-1}(z)$ is real number cannot be guaranteed over high frequency range, i.e. $R(\mathrm{e}^{j\omega T}) < 1$ may not be guaranteed when the frequency increases.

Considering this disadvantage of the conventional AFC, we propose to replace the single rate $\tilde{O}^{-1}(z)$ with a multirate discretization to attain a perfect inverse without considering whether the system is of minimum phase or not.

The stability properties of the AFC algorithm can be summarized as follows,

(1) It is exponentially stable if the transfer function $O(z)\tilde{O}^{-1}(z)$ is strictly positive real (SPR) [24]. The SPR condition requires that $O(z)\tilde{O}^{-1}(z)$ be stable and $R_e[O(j\omega)\tilde{O}^{-1}(j\omega)] > 0$ for all ω [63].

(2) When $O(z)\tilde{O}^{-1}(z)$ is not SPR, if $O(z)\tilde{O}^{-1}(z)$ is stable and the adaptation gain is sufficiently small, the adaptive algorithm is still stable [73].

Therefore the plant can be non-SPR, but the magnitude of the adaptation gain is limited. In other words, the convergence rate is limited for non-SPR systems.

3.3 Multirate Adaptive Feedforward Cancellation Scheme

To develop the multirate version of the AFC scheme, let T_r, T_u and T_y represent the period of reference input$r(t)$, control signal $u(t)$ and output measurement $y(t)$, respectively. Consider a nth-order single input single output (SISO) plant $P_c(s)$ described by

$$\begin{aligned} \dot{x}(t) &= A_c x(t) + B_c u(t), \qquad (3.30) \\ y(t) &= C_c x(t) + D_c u(t). \qquad (3.31) \end{aligned}$$

Its discrete-time model using generalized multirate sampling control ($T_f = T_r = NT_u = NT_y$) can be represented by

$$\begin{aligned} x[i+1] &= Ax[i] + Bu[i], \qquad (3.32) \\ y[i] &= Cx[i] + Du[i], \qquad (3.33) \end{aligned}$$

where $x[i] = x(iT_f)$, and $\left[\begin{array}{c|c} A & B \\ \hline C & D \end{array}\right] \triangleq$

$$\left[\begin{array}{c|cccc} A_s^N & A_s^{N-1}B_s & A_s^{N-2}B_s & \cdots & B_s \\ \hline C_s & D_s & 0 & \cdots & 0 \\ C_sA_s & C_sB_s & D_s & \cdots & 0 \\ \vdots & \vdots & \vdots & \cdots & \vdots \\ C_sA_s^{N-1} & C_sA_s^{N-2}B_s & C_sA_s^{N-3}B_s & \cdots & D_s \end{array}\right] \qquad (3.34)$$

where $P[z_s] = [A_s, B_s, C_s, D_s]$ is the plant discretized by zero order hold on $T_y(= T_u)$ and $z_s \triangleq e^{sT_y}$, $A_s = e^{A_c \frac{T_f}{N}}$, $B_s = \int_0^{T_f/N} e^{A_c \tau} B_c \mathrm{d}\tau$, $C_s = C_c e^{A_c \frac{T_f}{N}}$, $D_s = C_c \int_0^{T_f/N} e^{A_c \tau} B_c \mathrm{d}\tau$.

Such a system is a n-dimensional plant with N inputs and N outputs, with D being a square matrix of full rank. Thus we can get its inverse state-space model $\tilde{O}^{-1}(z) = \{A, B, C, D\}^{-1}$ directly:

$$\left[\begin{array}{c|c} A & B \\ \hline C & D \end{array}\right]^{-1} \triangleq \left[\begin{array}{c|c} A - BD^{-1}C & BD^{-1} \\ \hline -D^{-1}C & D^{-1} \end{array}\right] \tag{3.35}$$

As shown in Chapter 2, with the $\tilde{O}^{-1}(z)$ developed by multirate inverse, the phase of the shaped plant $O(z)\tilde{O}^{-1}(z)$ becomes zero over the whole frequency range. The SPR property of $O(z)\tilde{O}^{-1}(z)$ can be assured, thus the stability and effectiveness of convergence time of the AFC scheme are improved.

3.4 Summary

In this chapter, we retrospect several methods which are used to compensate disturbance in HDD servo system. After analyzing the strongpoint and weakness of these methods, we presented an adaptive feedforward compensator based on the proposed plant inverse scheme. Based on multirate discretization, we attain a more accurate inverse model of the closed-loop system regardless of the system being minimum phase or not, which is a critical step in the adaptive feedforward compensator design. Such a scheme will attenuate the RRO components in a wide range without amplifying other frequencies, which can not be achieved using the conventional AFC scheme. Next, simulation and experiment results will be given to show these benefits of the proposed scheme of dealing with disturbances in a HDD servo system.

Chapter 4

Application Example

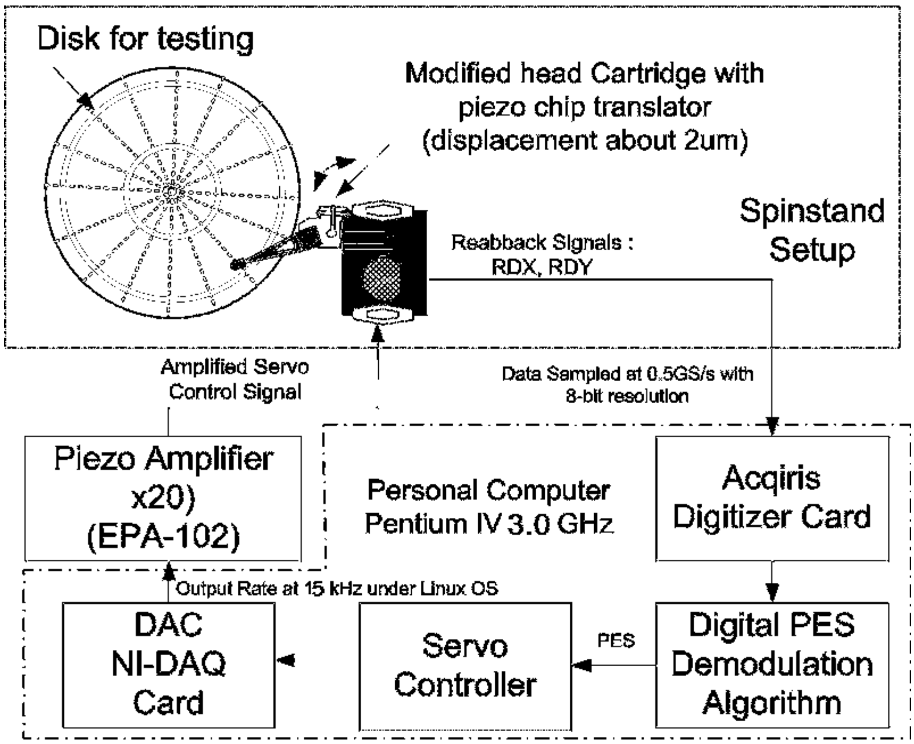

Figure 4.1: The block diagram of the spin stand servo system.

The scheme was applied to Spin Stand servo system as shown in Fig. 4.1. The spinstand is a system designed to mount and test HDD components (specifically heads, head stacks, disks, and channel, when used together with a read/write analyzer), simulating the conditions found in the actual HDD. In this paper, Guzik spinstand (Model S1701A) [53] is used to write servo patterns on the media. An Acqiris digitizer card (model: Acqiris DP210) is used to sample the read back signal at 0.5 GHz. A personal computer (PC) loads the data and calculates the PES. A National Instruments data acquisition (NI-DAQ) card (model: PCI-MIO-16E1) is used as the D/A convertor for the PC to send out control signal at 12 kHz. The output signal is amplified by a piezo amplifier and then is sent to control the PZT micro-actuator which moves the head [37]. The spindle rotation speed is set to 4000 rotation-per-minute (RPM), thus the basic frequency of the disturbance is 66.7 Hz. We'll see later in the experiment that such a system, which is more accessible than HDDs, also has abundant RRO components similar to HDDs, and thus used as our testing platform.

To move the read/write head of precision motion control, a low voltage piezo chip translator (LVPZT) (Model No. PL033) [81] with displacement range of 2 mm and resolution of 0.02 nm is used as the positioning device to drive the suspension. The controlled plant is thus having three components: the PZT translator chip, the head cartridge base and a non-active suspension with the read head.

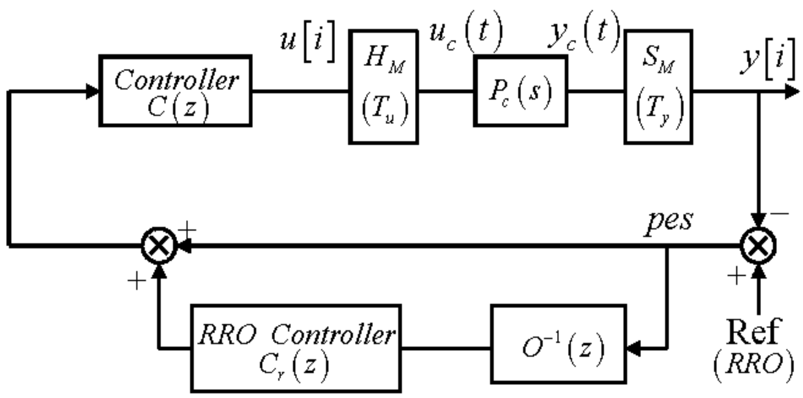

Figure 4.2: Block diagram of the servo system.

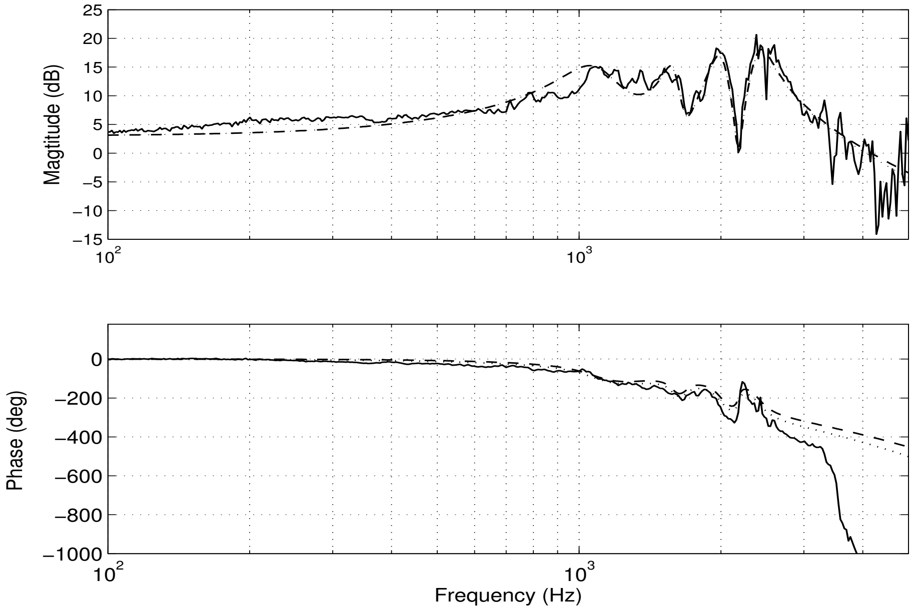

Figure 4.3: Frequency response and identified model
of the PZT micro-actuator with head cartridge.

From the measured frequency response shown in Fig. 4.3, the plant $P_c(s)$ for the PZT actuator is a 9-th order model measured using a Dynamic Signal Analyzer (model: Hewlett Packard 35670A) given by:

$$P_c(s) = \prod_{i=1}^{9} k \frac{s - z_i}{s - p_i} \tag{4.1}$$

with $z_i = (-2.4734, -1.2566, -0.0399,\ -0.0021 \pm 0.1368i,\ -0.0042 \pm 0.1055i,\ -0.0150 \pm 0.0819i) \times 10^{-5}$, $p_i = (-1.2566\ -0.0833 \pm 1.5120i,\ -0.0603 \pm 1.2552i\ -0.0398 \pm 0.9951i,\ -0.0953 \pm 0.6738i) \times 10^{-4}$, and $k = 0.0165$. The plant is discretized using ZOH method at a sampling frequency of 15 kHz.

The block diagram of the whole system is shown in Fig. 4.2. The controller $C(z)$ is a simple lag-lead type compensator $(\frac{0.2z^2}{z^2 - z})$ in cascade with an approximate inverse model of the plant as a pre-compensator $C_2(z)$:

$$C_2(z) = \prod_{i=1}^{9} k \frac{z - z_i}{z - p_i}, \tag{4.2}$$

with $k = 0.634$, $z_j = 0.4327$, $0.5048 \pm 0.8001i$, $0.6434 \pm 0.7132i$, $p_j = (0.8454 \pm 0.4075i\ ,\ 0.7673 \pm 0.5997i) \times 10^{-5}$, $0.00023, 0.7664, 6.9 \times 10^{-8}$, $0.6037 \pm 0.7801i$, $0.7416 \pm 0.6287i$, $0.7734 \pm 0.4699i$. With such a control scheme, the closed-loop system has a -3 dB cut-off of around 1020 Hz which can be represented by a reduced order model $\frac{0.06s+1201}{1.06s+1211}$ using low order model curve fitting method.

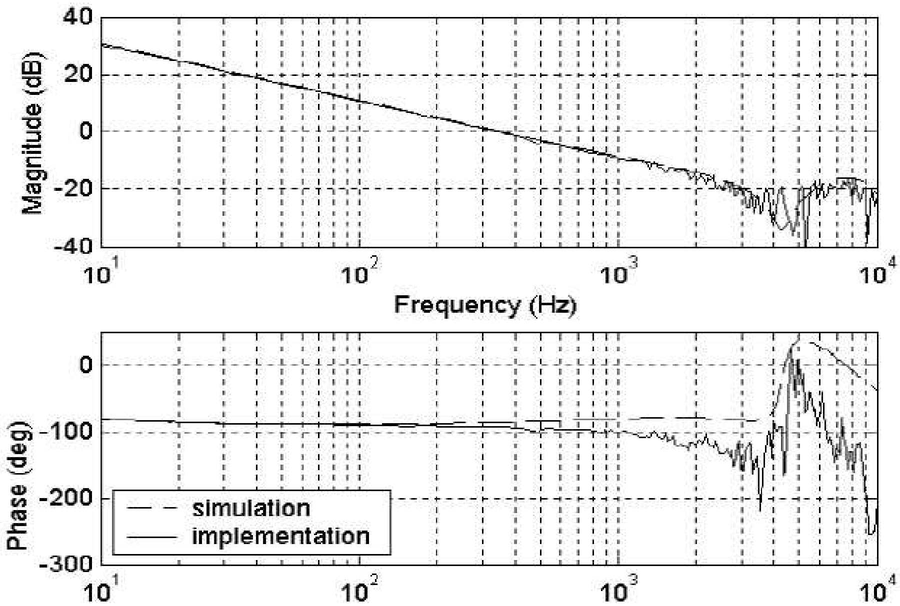

Figure 4.4: Frequency response of the controller.

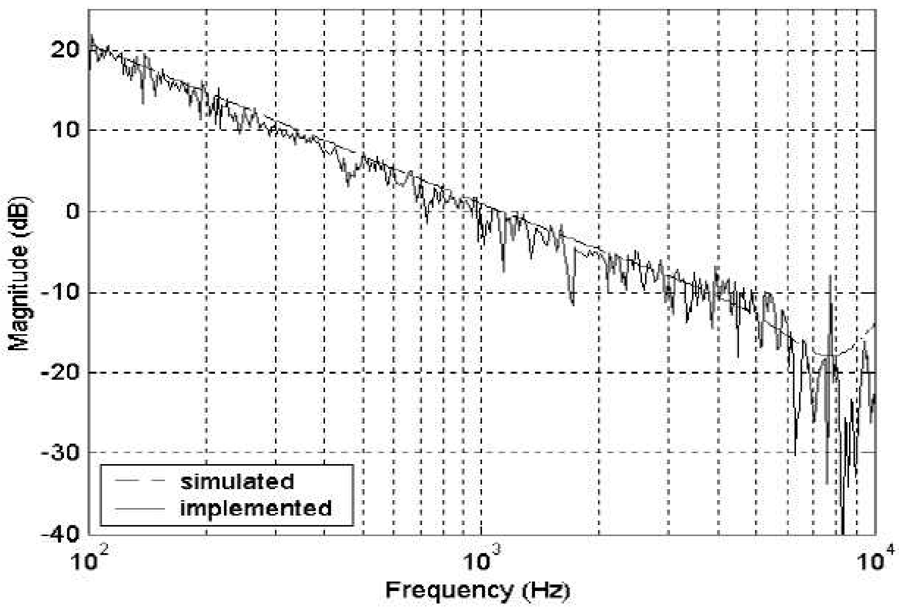

Figure 4.5: Frequency response of the open loop.

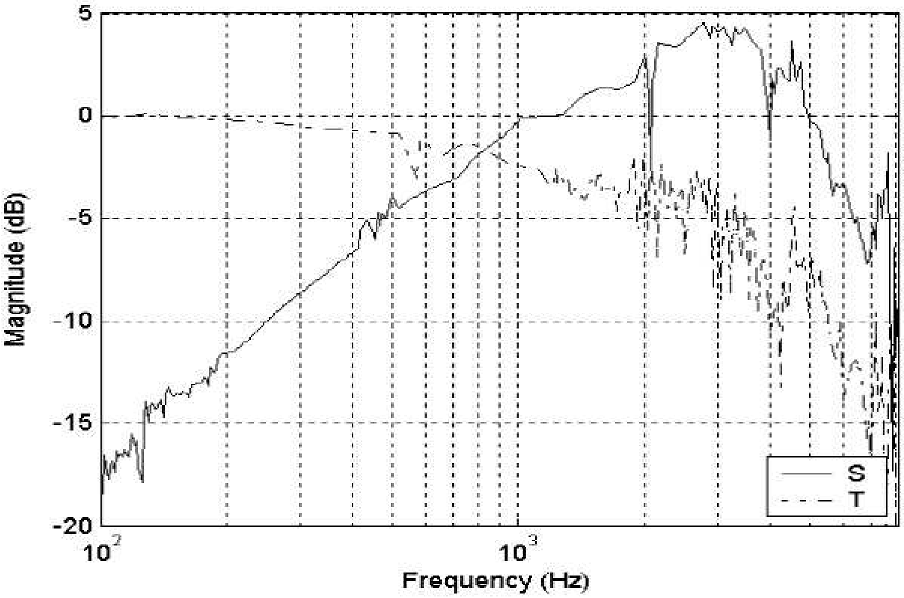

Figure 4.6: Frequency response of sensitivity and closed-loop transfer functions.

Fig. 4.4 and Fig. 4.5 show the frequency response of the designed controller $C(z)$ and the compensated open loop $C(z)P_c(z)$ respectively. Fig. 4.6 shows the frequency response of sensitivity and closed-loop transfer functions.

Next, we will compare two schemes: 1), the conventional AFC scheme ($1/T_r = 1/T_u = 1/T_y = 15$ kHz), where $\tilde{O}^{-1}(z)$ is obtained using equation (3.29), and thus $\tilde{O}^{-1}(z) = \frac{z-0.9267}{0.057z+0.016}$, and 2), the proposed scheme ($1/T_r = 1/(2 \times T_u) = 1/(2 \times T_y)$= 15 kHz), with $\tilde{O}^{-1}(z) = \{A, B, C, D\}^{-1}$ is obtained using equation (2.16) and thus, $\tilde{O}^{-1}(z)$= $\left[\begin{array}{c|c} A & B \\ \hline C & D \end{array}\right]^{-1}$ =

$$\left[\begin{array}{c|cc} 6.2458e-008 & -3.9977e-006 & 0.015996 \\ \hline -625 & 10 & 0 \\ 0.1562 & -9.9975 & 10 \end{array}\right] \tag{4.3}$$

Fig. 4.7 shows the magnitude of $R(\mathrm{e}^{j\omega T})$ when we select the RRO components at 66.7, 266.8, 466.9 Hz to be cancelled out using the AFC scheme. The

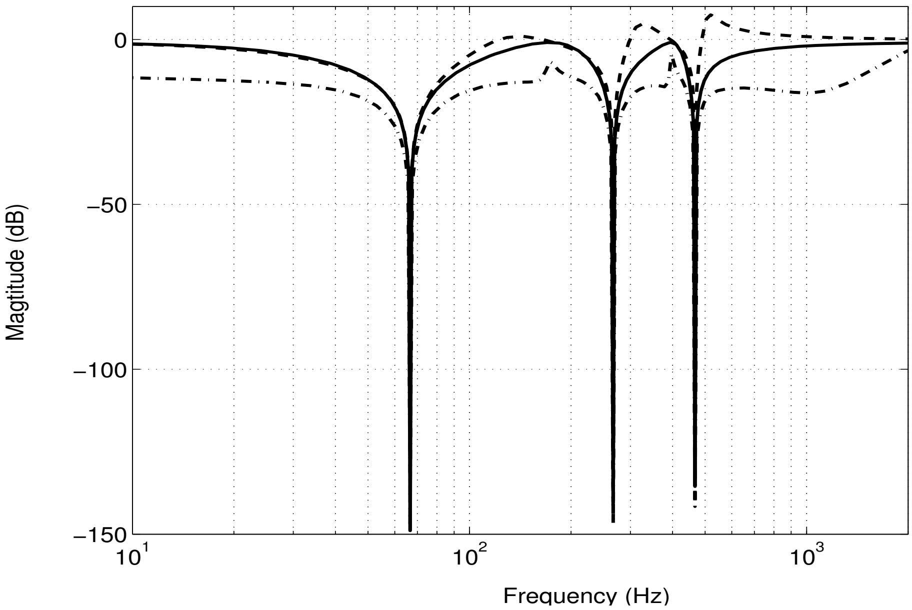

Figure 4.7: The magnitude of $R(s)$ with runout compensators at $\omega_i = 66.7$ Hz, 266.8 Hz and 466.9 Hz. The solid line shows the case assuming $O(z)\tilde{O}^{-1}(z) = 1$; The dashed line shows the case of conventional AFC scheme with $\tilde{O}^{-1}(z)$ calculated by equation (3.29); The dash-dot line shows the proposed scheme with $\tilde{O}^{-1}(z)$ calculated by equation (4.3). The $|R(\mathrm{e}^{j\omega T})|$ of conventional AFC has greater than 0-dB gain at frequencies at 133.4, 333.5 and 533.6 Hz and thus will amplify the RRO components at those frequencies.

figure shows that the proposed multirate compensation scheme will attenuate the RRO components at the desired frequencies without amplifying the RROs at other frequencies. With bigger adaptive gain, the attenuation will be further while sacrificing the stability. Thus the adaptive gain is set as the marginal highest value in the conditions of keeping the whole system stable.

4.1 Dual-frequency PES Formulation

The default servo pattern within the Spinstand is based on amplitude detection which has been widely used to determine the off-track position of the read/write head with respect to the disk media [6]. In this thesis, multiple-frequency servo pattern written at narrower than writer width is chosen for the servo pattern layout on the spin stand as shown in Figure 4.8. Such a pattern requires less servo overhead and is easy to determine the sign of the PES. In addition, it is not as sensitive to the effect of timing jitter as the phase servo pattern [62].

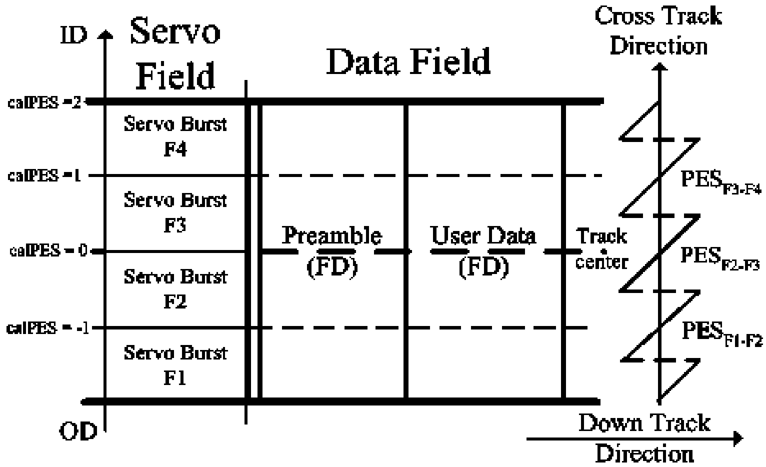

Figure 4.8: Multiple-frequency servo burst pattern.

4.1.1 Discrete Fourier Transform Detection of PES

A method based on discrete Fourier transform (DFT) algorithm can be used to extract the amplitude of each of these frequency components and generate PES, since the encoded position pattern contains different servo frequencies components [6]. Comparing with coherent detection using selective harmonics [3], DFT-based method is more robust against timing jitter [91].

The DFT equation is as follows:

$$\begin{aligned}
D(k) &= \sum_{n=0}^{N-1} x(n) W_N^{nk}, \\
&= \sum_{n=0}^{N-1} x(n) e^{-j\frac{2\pi nk}{N}}, \\
&= \sum_{n=0}^{N-1} x(n)[\cos\frac{2\pi nk}{N} - j\sin\frac{2\pi nk}{N}],
\end{aligned} \tag{4.4}$$

The estimated amplitude of F_i (i=1, 2) servo burst is

$$\begin{aligned}
D_i &= \sum_{n=1}^{N*p} S_1(n) \times e^{-j2\pi(n-1)/N}, \\
&= D_{ireal} - jD_{iimg}, \\
|D_i| &= \frac{[(D_{ireal})^2 + (D_{iimg})^2]^{1/2}}{D_{fni}}.
\end{aligned} \tag{4.5}$$

where $S_i(n)$ $(i = 1, 2)$ are the re-sampled servo signal $x(n)$ according to the sampling points per cycle of the servo frequencies F_1 and F_2 respectively. D_{fn1} and D_{fn2} are the factors to normalize the magnitude of each frequency components. Similar to the previous demodulation techniques, the position error is computed as

$$PES_{F1-F2} = \frac{|D_1| - |D_2|}{|D_1| + |D_2|} \tag{4.6}$$

where PES_{F1-F2} is the measured off-track result with respect to the center of the servo track.

4.1.2 Calibration of PES

In this setup, servo pattern of four different frequencies are written on the 2.5" magnetic disk to represent four servo tracks of 10 μinch for demonstration of track following operation.

The written servo pattern frequency are chosen to be $F_1 = 31.25$ MHz, $F_2 = 25$ MHz, $F_3 = 20$ MHz and $F_4 = 12.5$ MHz respectively. The sampling rate of the digitizer card is set at 500 MHz, and the number of sample points is 400, which means the frequency resolution for the DFT would be 1.25 MHz.

Theoretically, there are often positioning offset error due to the differences in the amplitude of the readback servo signal at different frequencies. Thus the computed individual frequency cross-track functions are normalized to eliminate the positioning offset errors.

$$\begin{aligned} G_{n1} &= \frac{G_1}{(G_1 + G_2 + G_4)} \\ G_{n2} &= \frac{G_2}{(G_1 + G_2 + G_3)} \\ G_{n3} &= \frac{G_3}{(G_2 + G_3 + G_4)} \\ G_{n4} &= \frac{G_4}{(G_3 + G_4 + G_1)} \end{aligned} \tag{4.7}$$

Using (4.7), each individual frequency components, $|D_x|$ where $x = 1, 2, 3, 4$ are normalized and Figure 4.9 shows the individual normalized frequency components, G_{n1} of F_1, G_{n2} of F_2, G_{n3} of F_3 and G_{n4} of F_4 using Goertzel detection technique respectively.

These individual DFT components of the servo pattern are calibrated and combined to form a suitable position signal to be fed into the servo controller. The calibrated PES, P_{cal} is formed by combining the valid region of each individual

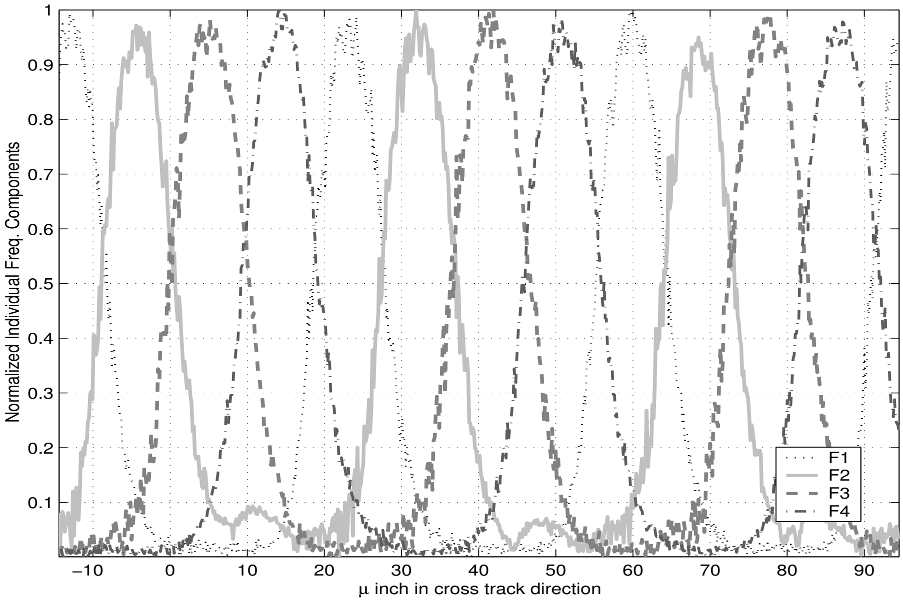

Figure 4.9: Normalized Goertzel computation of servo pattern F_1, F_2, F_3 and F_4.

dual-frequency PES, P_{Fn} where $F = 1, 2, 3, 4$ as follows:

$$\begin{aligned} P_{F1-F2} &= \frac{(G_{n1} - G_{n2})}{(G_{n1} + G_{n2})}, \\ P_{F2-F3} &= \frac{(G_{n2} - G_{n3})}{(G_{n2} + G_{n3})}, \\ P_{F3-F4} &= \frac{(G_{n3} - G_{n4})}{(G_{n3} + G_{n4})}, \\ P_{F4-F1} &= \frac{(G_{n4} - G_{n1})}{(G_{n4} + G_{n1})}, \end{aligned} \tag{4.8}$$

$$P_{cal} = \begin{cases} -sP_{F1-F2} - s_1; & \text{at -150 \% to -50\% of tc} \\ -sP_{F2-F3}; & \text{at -50 \% to -50\% of tc} \\ -sP_{F3-F4} + s_1; & \text{at +50 \% to +150\% of tc} \\ -sP_{F4-F1} + s_2; & \text{at +150 \% to +250\% of tc} \\ invalid & \text{out of range} \end{cases} \tag{4.9}$$

where $s_1 = 1.0$ and $s_2 = 2.0$ are the PES magnitudes with respect to the track width and track center t_c, respectively. Since 1 unit is chosen to correspond to 1 track width, the *scale* factor, s is set to be 0.5 as the individual PES range from

-1 to 1.

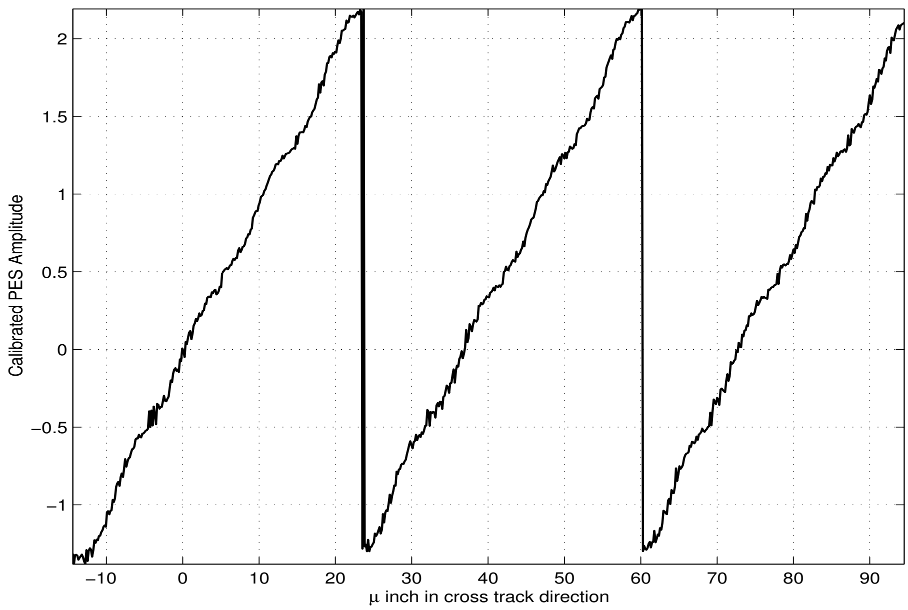

Figure 4.10: Calibrated PES function.

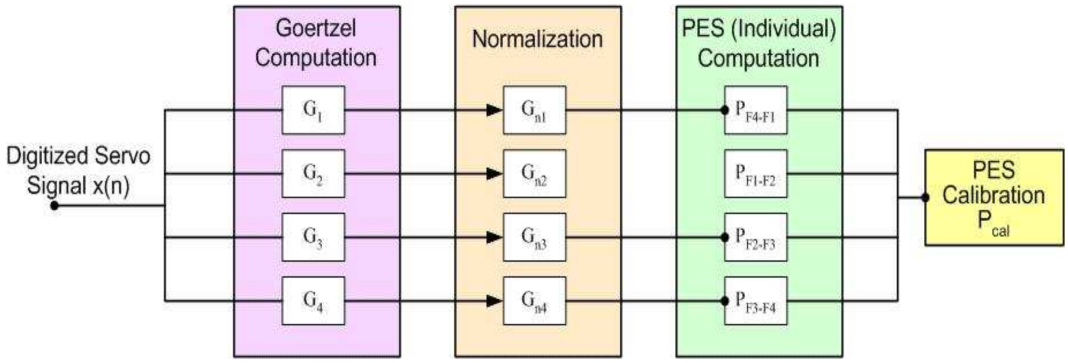

Figure 4.11: Block diagram of PES generation and calibration process.

Based on (4.9), the extended PES is as shown in Figure 4.10. An overview of the PES demodulation process is as shown in Figure 4.11.

Next, the control convergence time under various conditions, robustness against plant parameters, as well as the loops behavior under experimental conditions will be given.

4.2 Comparison of convergence time

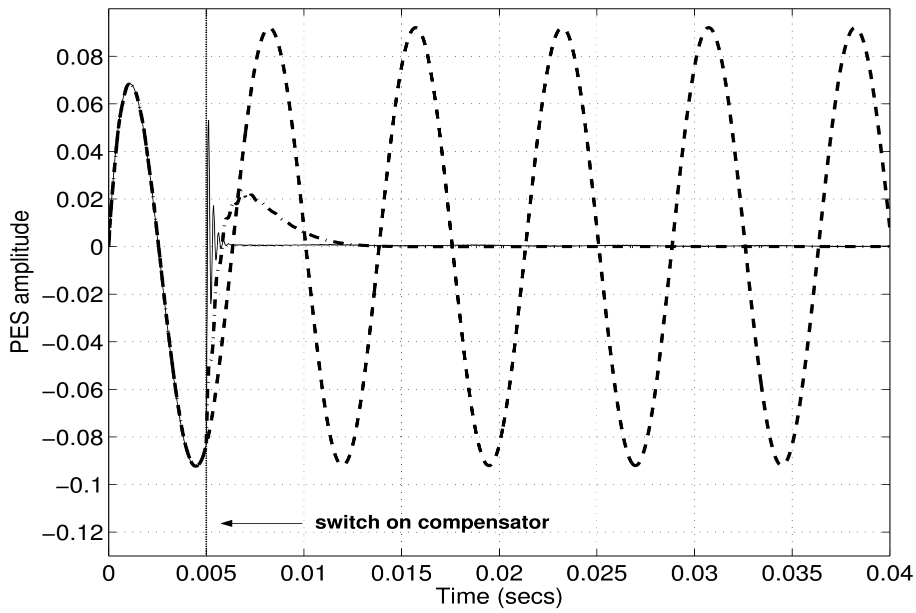

Figure 4.12: The PES signal with single frequency RRO. Dashed line: without AFC compensation; dash-dot line: conventional AFC scheme with a convergence time of 20 ms; solid line: the multirate AFC scheme with a convergence time of 13 ms.

Fig. 4.12 shows the time domain PES signal with RRO signal at 133.4 Hz when applying the conventional and multirate AFC schemes. The upper bond of the adaptation gain is determined by the stability of the system which can be calculated from the Nyquist plot. In both schemes, the convergence time begins to increase when the adaptation gain is bigger than certain values. The adaptation gain which results in minimum convergence time is set to be $g_1 = 1.1$ in conventional scheme and $g_1 = 3$ in multirate scheme respectively. When using the conventional AFC scheme, the PES signal converges to zero in 0.008 second; when using the proposed scheme, the PES signal converges to zero in 0.003 second which is 63% shorter.

Fig. 4.13 presents the simulation results of the PES signal with multiple frequency RRO input at $\omega_i = 66.7$, 266.8 and 466.9 Hz respectively when applying

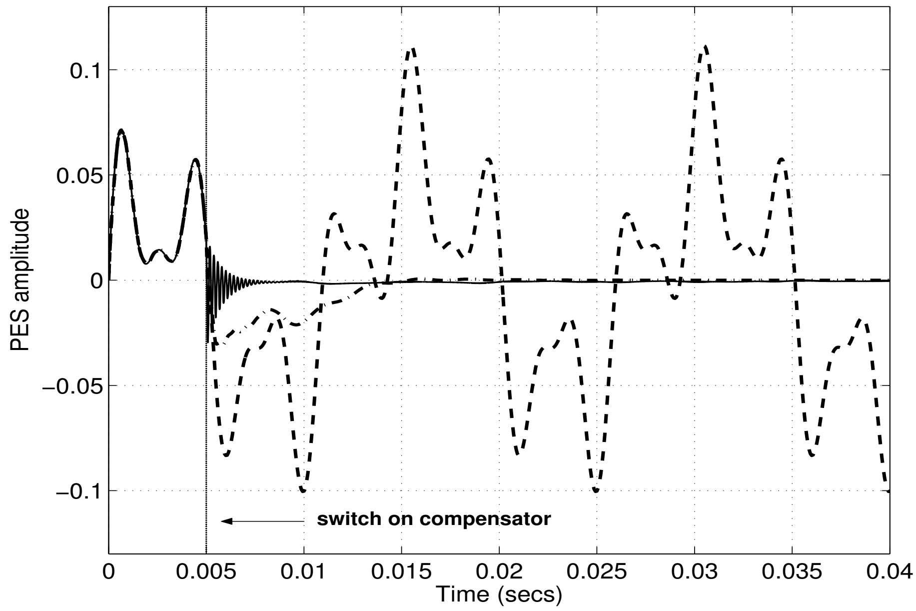

Figure 4.13: The PES signal with multiple frequency RRO. Dashed line: without AFC compensation; dash-dot line: conventional AFC scheme with a convergence time of 10 ms; solid line: multirate AFC scheme with a convergence time of 5 ms.

the two schemes. The adaptation gains which result in minimum convergence time are set to be 0.4, 0.1, 0.1 in conventional scheme and 1, 2, 2 in proposed scheme respectively. When using the conventional AFC scheme, the PES signal converges to zero in 0.01 second; while when using the proposed scheme, the PES signal converges to zero in 0.005 second which is 50% shorter.

To test the system's response against periodic vibrations of known frequencies and time varying amplitude, Fig. 4.14 shows the responses of the system with the two schemes. In Stage 1, the disturbance is a sine wave with frequency of 66.7 Hz and amplitude of 0.08 μm. In Stage 2, the frequency changed to 90 Hz and amplitude changed to 0.16 μm linearly with respect to time. In Stage 3, the amplitude and frequency fixed at 0.16 μm and 90 Hz respectively. Using the same scheme as described previously plus the knowledge of the runout signal frequency, the proposed scheme converges the PES signal to zero 10% faster than the normal

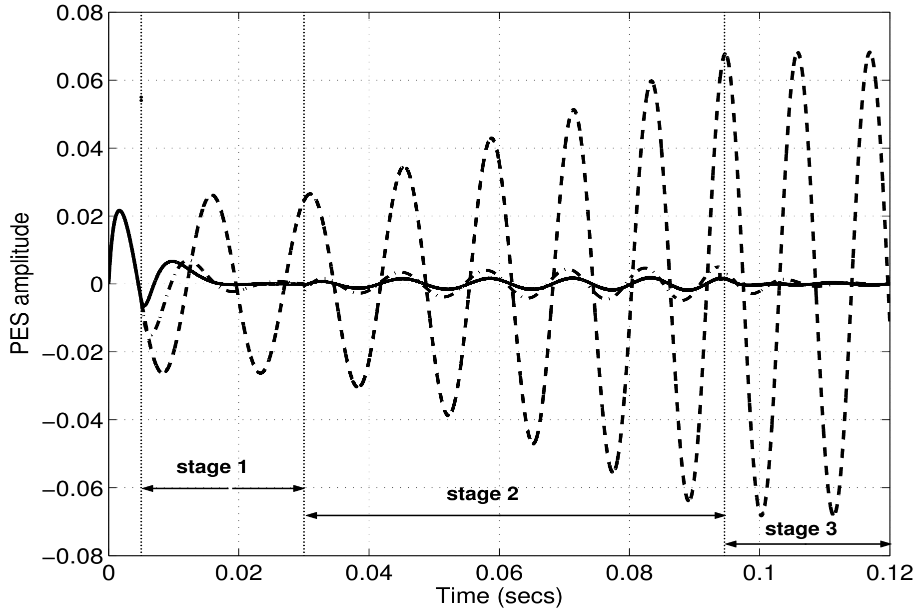

Figure 4.14: The PES signal with a time-varying RRO. Dashed line: without AFC compensation; dash-dot line: with conventional AFC scheme; solid line: with multirate AFC scheme.

AFC scheme in Stages 1 and 3. In Stage 2, the proposed scheme reduces the PES to 1.8×10^{-3} μm which is 40% less than the usual AFC scheme which reduces the PES signal to 3×10^{-3} μm.

Fig. 4.15 shows the process that the two schemes follow and cancel another time-varying disturbance signal. In Stage 1, the disturbance is a sine wave with fixed frequency 133 Hz and amplitude 0.08 μm. In Stage 2, the frequency changed to 100 Hz and amplitude changed to 0.04 μm linearly with respect to time. In Stage 3, the amplitude and frequency are fixed at 0.04 μm and 100 Hz respectively. Assuming the frequency of disturbance can be measured, we keep the frequency in the adaptive algorithm as the same as the frequency of disturbance. In Stage 1 and 3, the proposed scheme converge PES signal to zero 15% faster than the normal AFC scheme. In Stage 2, the normal AFC scheme reduces the PES signal to 2.6×10^{-3} μm, while that of the proposed scheme is 0.9×10^{-3} μm which is 65%

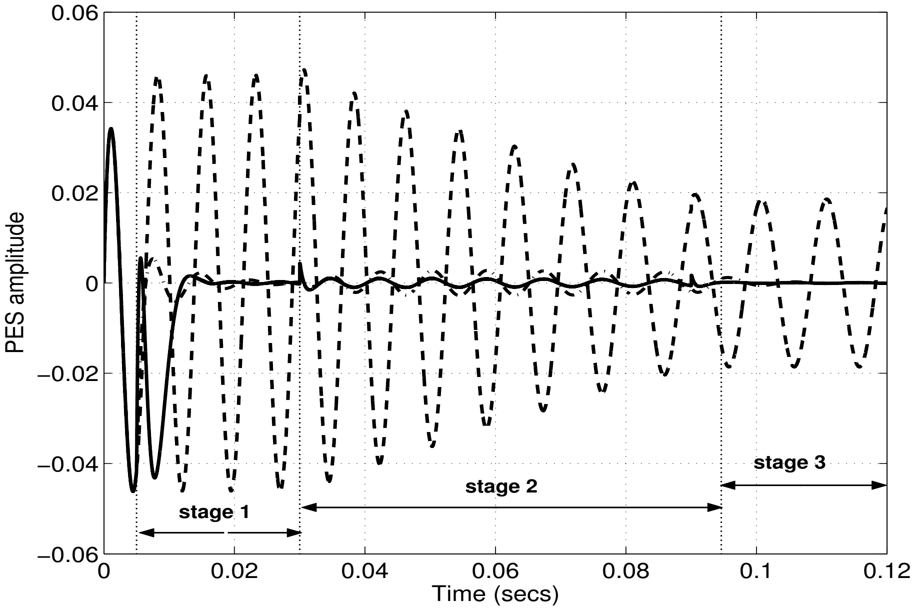

Figure 4.15: Simulation results: The PES signal with time-varying RRO (dashed line: without AFC compensation; dash-dot line: with conventional AFC scheme; solid line: with multirate AFC scheme).

less.

Such a result shows that the proposed scheme is more effective in time-varying runout compensations, such as in variable speed hard disk drives, or disk drives with a varying external disturbance such as those mounted in an automobile.

4.3 Robustness against actuator parameter uncertainty

Fig.4.16 shows the PES signal with and without the proposed compensator when the first three resonant modes shifted 10% lower. From this picture, we can see that even with such an uncertainty, the system is still stable and achieved a 40 dB attenuation of the RRO.

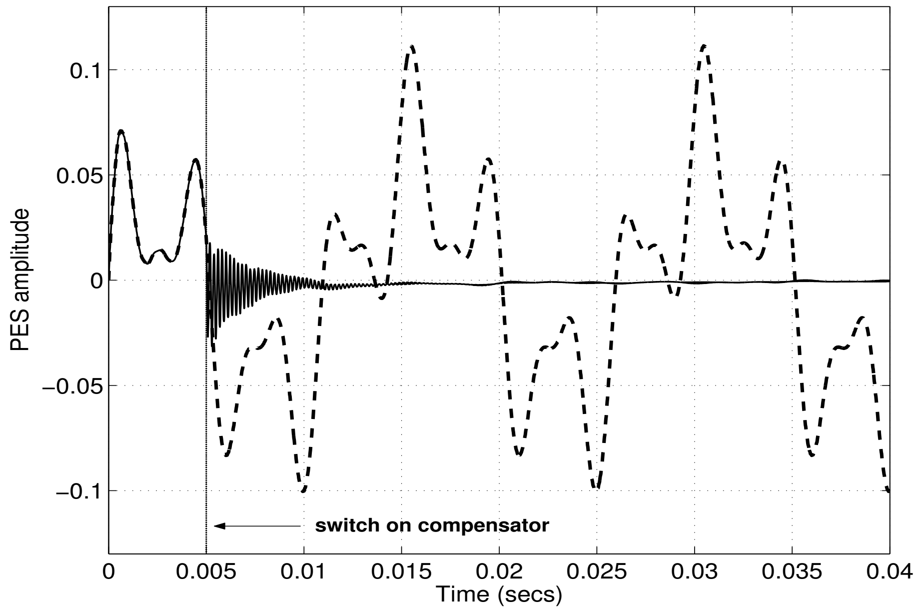

Figure 4.16: The PES signal with actuator uncertainty using the proposed scheme.

4.4 Experiment results

Fig. 4.17 shows the PES power spectrum with and without feedback control. With feedback control scheme (without AFC compensator), the first and second RRO frequencies which contribute most to the PES spectrum have already been attenuated.

Fig. 4.18 presents how the two AFC schemes attenuate RRO harmonics. We select the 1st, 2nd, 7th, 13th, 30th, and 32th harmonics, i.e. 66.7, 133.4, 466.9, 867.1, 2001, and 2134.4 Hz, to compensate. Fig. 4.19 compares the RRO reduction rate corresponding to Fig. 4.18. We can see from these figures that

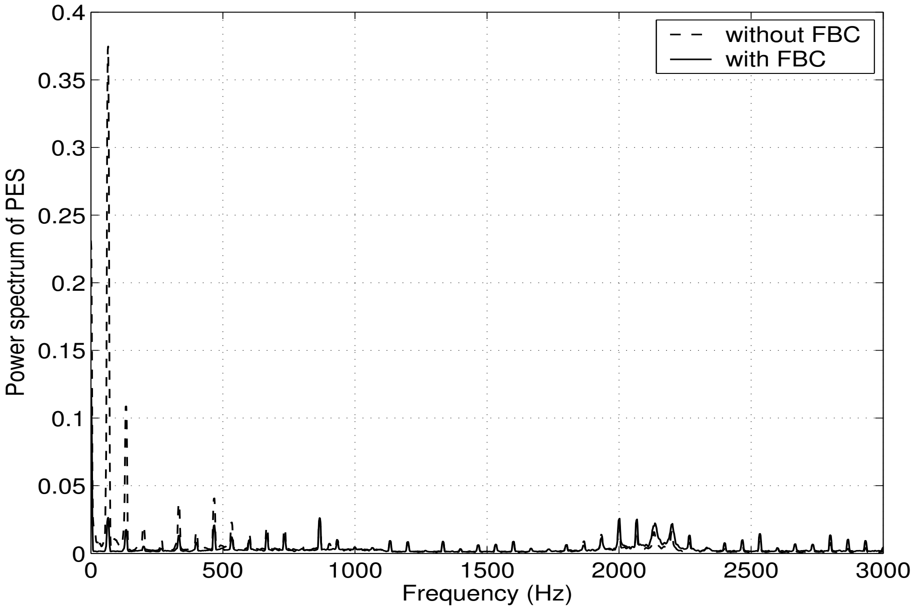

Figure 4.17: The PES power spectrum with and without Feedback Control (FBC).

the conventional scheme can attenuate lower frequency harmonics quite a lot but it can not attenuate higher frequency harmonics as effectively; furthermore, it even amplifies some harmonics around 2 kHz. The proposed scheme can attenuate selected harmonics over a very wide frequency range without amplification.

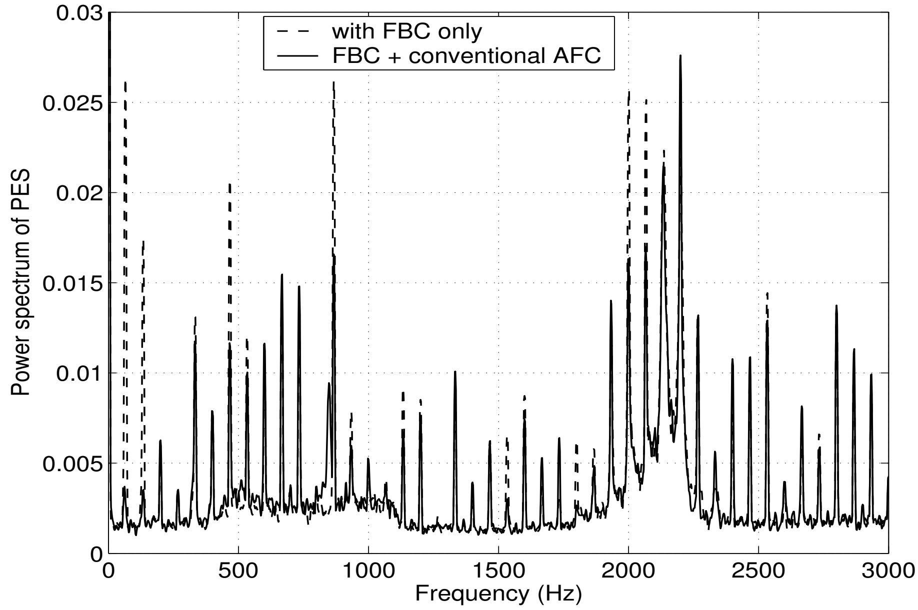

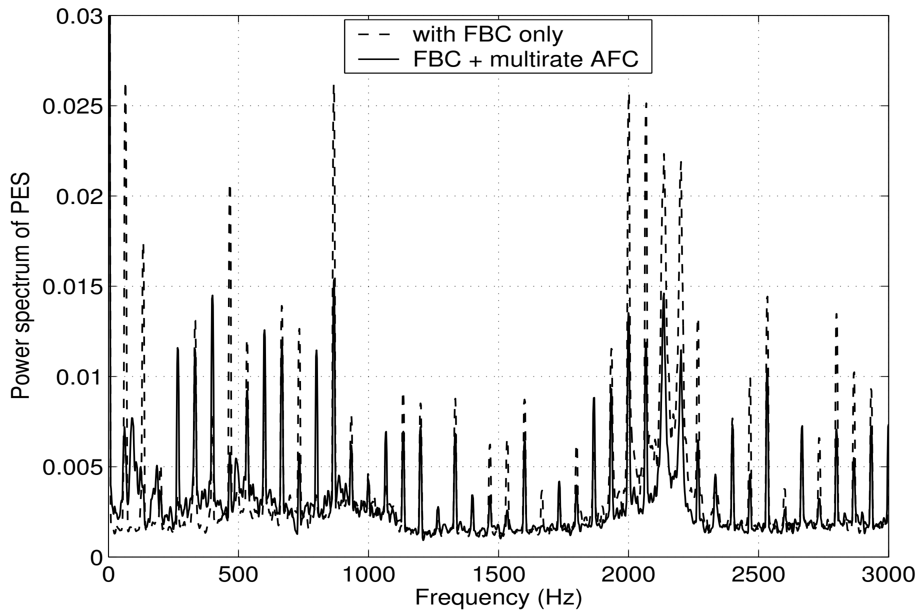

Figure 4.18: The PES power spectrum obtained from experiment results. We selected the 1st, 2nd, 7th, 13th, 30th and 32th harmonics to be compensated. The conventional AFC scheme brings down the PES 3σ by 23.7% while the proposed scheme brings down the PES 3σ by 25%.

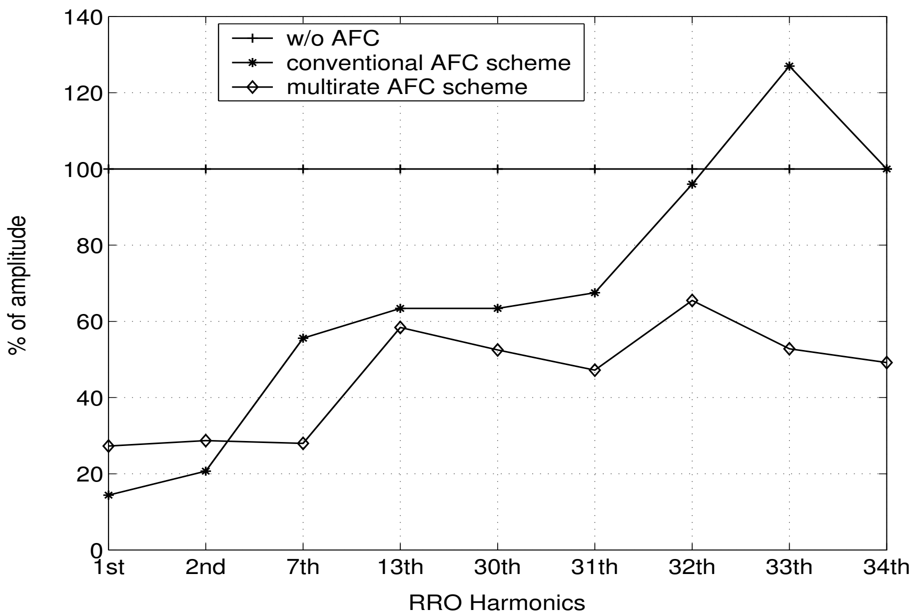

Figure 4.19: RRO reduction rate comparison of the two schemes. The conventional AFC can not attenuate the RROs at 7th, 13th, 30th and 32th harmonics as effectively as the proposed multirate scheme, and further amplifies the 33th RRO harmonic.

Chapter 5

Conclusions and Future Work

This thesis focuses on the periodic disturbance compensator designs for HDD servomechanism to achieve robust periodic disturbance cancellation over a wide frequency range. Different kinds of periodic disturbance compensators including internal model based repetitive control algorithms and conventional AFC scheme are investigated. A new multirate based AFC scheme is proposed. The comparison of the proposed scheme and conventional schemes in both simulation and experiment results show that the proposed scheme performs better than the conventional scheme in convergence time, high frequency harmonics cancellation and robustness.

The following research work has been done in the dissertation:

(i) To design the servo system under limited sampling frequency, the thesis considered multirate control designs. After reviewing the multirate control system theory and its application HDD servo system, we proposed an plant inverse scheme based on multirate sampling and inverse. The comparison between the proposed scheme and conventional scheme is made in Chapter 2. With multirate discretization, we can attain a inverse model of the plant without considering the unstable zero issue and the shaped plant with multirate inverse has more zero phase feature than the shaped plant obtained by the usual plant inverse scheme.

(ii) To further improve the control system performance against periodic disturbance including RRO, external periodic vibration and even time varying periodic disturbance, we presented an adaptive feedforward compensator based on the proposed plant inverse scheme. We compare the proposed scheme with conventional AFC scheme in Chapter 3. Based on multirate discretization, we attain a more accurate inverse model of the closed-loop system without considering whether the system is of minimum phase or not which is a critical step in the adaptive feedforward compensator design. We've shown that such a scheme will attenuate the RRO components in a wide range without amplifying other frequencies, which can not be achieved using the conventional AFC scheme.

(iii) An application example of applying the proposed scheme to spin stand servo system is given in Chapter 4. Simulation and experiments results have confirmed the analysis results above, and also shown that the proposed scheme can reduce the PES signal more rapidly even when the disturbance signal is a time-varying one. The scheme is also robust against plant parameter various.

In view of the results obtained, the following work should be emphasized in future research:

1. Consider other multirate sampling case.

   In the thesis, only one of the multirate sampling cases is investigated. In the cases including systems with special hardware restrictions such as visual servo systems, and so on, the sampling of output signal may be restricted by the hardware thus cannot be assumed to be as fast as the sampling of control input. Thus We may consider the case $T_y > T_x$ to further improve the scheme from both theory and application point of view.

In the case $T_f = T_y = NT_u = MT_x$, although T_y is decided in advance, the plant input can be changed N times during T_y. In this case, the perfect tracking control can be assured M ($\triangleq N/n$) times during intersample points of T_y, as shown in Fig. 5.1. Fig. 5.2 shows the proposed multirate control scheme, in which the plant input is changed N times during one frame period T_f, and the plant output is also detected M times during T_f. The positive integers M and N indicate input and output multiplicities, respectively.

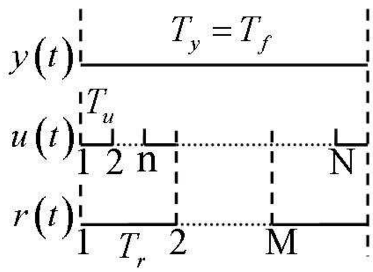

Figure 5.1: Multirate sampling case 2.

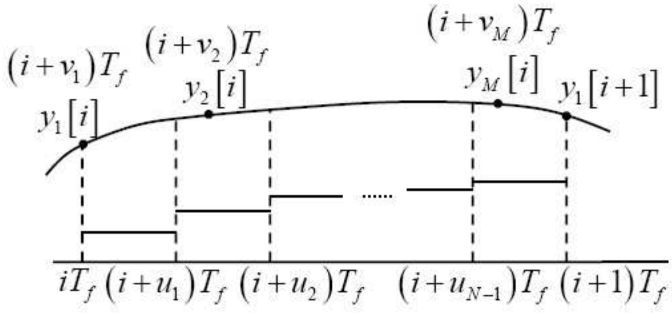

Figure 5.2: Generalized multirate sampling.

Fig. 5.3 presents the structure of the proposed controller for case2.

2. Find more effectiveness algorithms to suppress time-varying periodic vibra-

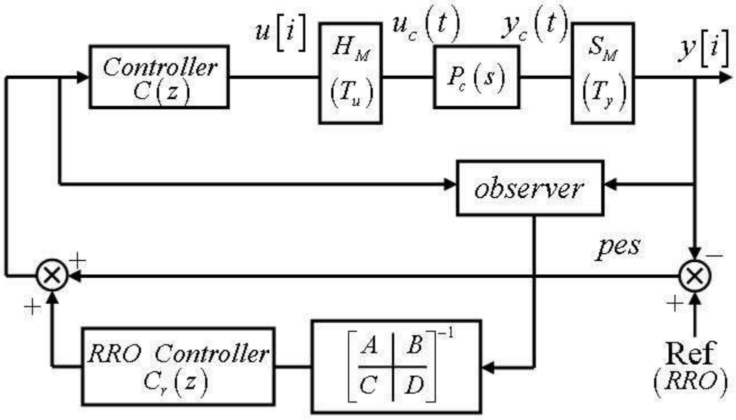

Figure 5.3: Structure of the proposed controller for Case 2.

tions both internal and external to the hard disk drives.

The proposed scheme discussed in this thesis has better reduction of the time-vary periodic vibrations when compared with conventional schemes. We believe by modifying the adaptive algorithm, we can track frequency varying periodic disturbance more accurately and finally eliminate them.

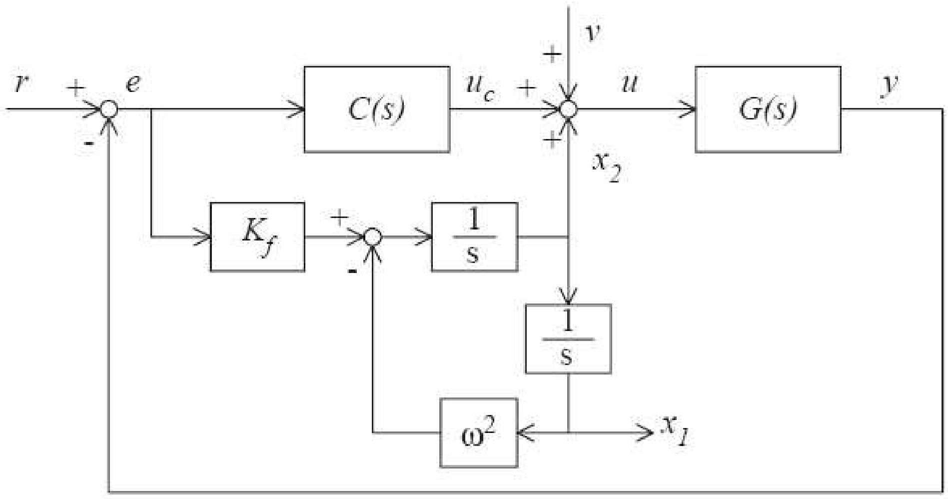

Figure 5.4: The block diagram of an internal model control system.

A simple integral controller can be used to convert the measurement of ω_c into a constantly updated ω. The error ε between the $\hat{\omega}_c$ and ω can be

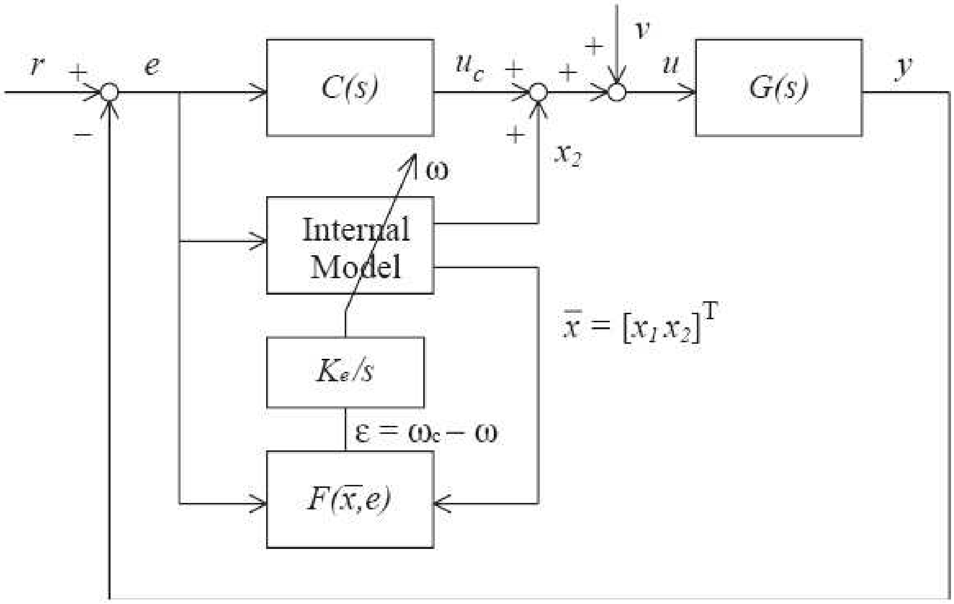

Figure 5.5: The block diagram of an adaptive cancellation control system.

expressed as follows:

$$\varepsilon = \hat{\omega}_c - \omega, \tag{5.1}$$

and ω can be updated by

$$\frac{d\omega}{dt} = -K_e\varepsilon = -K_e\frac{\omega K_f e x_1}{(\omega x_1)^2 + x_2^2}, \tag{5.2}$$

where K_e is a small constant gain. Fig. 5.5 shows the structure of the adaptive cancellation control system we use in this paper.

The scheme above can be used to track and cancel periodic disturbance with uncertain frequency, while how to cancel the periodic disturbance with varying amplitude still worth to be considered.

With improved design, we will test the scheme on speed-variable HDDs to further investigate the advantages and disadvantages of the proposed scheme. Because currently we only test the effectiveness of the proposed scheme when dealing with time-varying periodic disturbance using simulation, if experiment can be done, the characteristic of the proposed scheme can be further validated.

3. Extend the scheme to deal with narrow-band disturbances.

   As we mentioned in Section 1.2.2, the solution to reject narrow-band disturbances need to be further studied. As high adaptation gain need to be applied because of the rapid variation of amplitude and phase of the non-synchronous disturbance, the sluggish transient response caused by the big adaptation gain should be the problem.

   In mode-switching control scheme in HDD, Initial Value Compensation (IVC) is used to improve the transient response after switching from seeking mode to tracking mode. The same idea can be used to improve transient response in the proposed disturbance cancellation scheme. The basic concept is shown in Fig. 5.6.

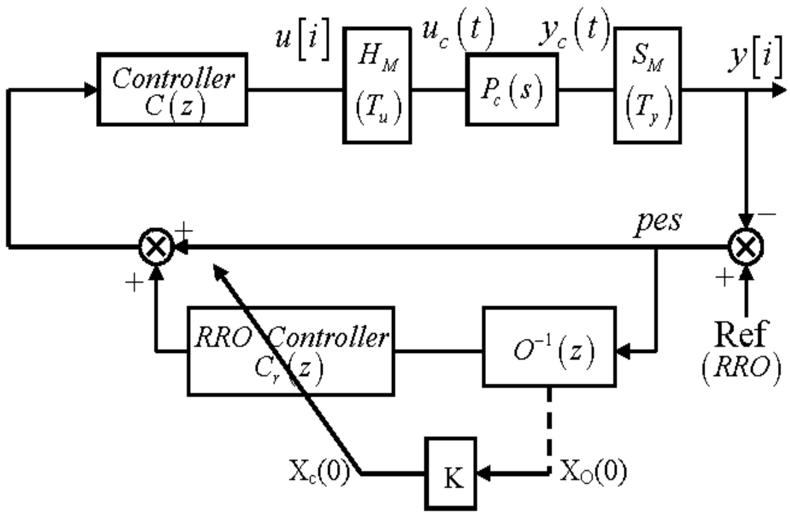

Figure 5.6: The proposed scheme with IVC.

   To avoid the phase loss introduced by the zero order holds which are used to obtain intersample signal, the intersamper observer can be considered in the design process.

Bibliography

[1] Abramovitch, D., T. Hurst, and D. Henze, "Decomposition of baseline noise sources in hard disk position error signals using the PES pareto method," *Proc. American Control Conf.*, Jun. 1997, New Mexico, USA, pp. 2901-2905.

[2] Abramovitch, D., "Rejecting rotational disturbances on small disk drives using rotational accelerometers," *Contr. Eng. Practice.*, Vol.5, Nov. 1997.

[3] Abramovitch, D., "Customizable coherent servo demodulation for disk drives," *IEEE/ASME Trans. Mechatronics*, Vol. 3, No. 3, pp. 184-193, Sep. 1998.

[4] Abramovitch, D. and G. Franklin, "A brief history of disk drive control," *IEEE Control Systems Magazine*, Vol. 22, No. 3, pp. 28-42, Jun. 2002.

[5] Albertos, P., "Block multirate input-output model for sampled-data control systems," *IEEE Trans. Automat. Contr.*, Vol.35, No. 9, pp. 1085-1088, 1990.

[6] Al-Mamun, A., T.H. Lee, G. Guo, W.E. Wong, and W. Ye, "Measurement of position offset in hard disk drive using dual frequency servo bursts," *IEEE Trans. Instrumentation and Measurement*, Vol. 52, No. 6, pp. 1870 - 1880, Dec. 2003.

[7] Al-Rahmani, H. M., "A new design method for multirate digital controls," Ph.D thesis, Stanford University, 1991.

[8] Al-Rahmani, H. M. and G. F. Franklin, "Multirate control: a new approach," *Automatica*, Vol. 28, No. 1, pp. 35-44, 1992.

[9] Amit, N. and J. D. Powell, *Optimal digital control of multirate systems*, American Institute of Aeronautics and Astronautics, pp. 423-429, 1981.

[10] Aracil, R. and V. Feliu, "Multirate sampling technique in digital control systems simulation," *IEEE Trans. Sys., Man. and Cybernetics*, Vol. 14, No. 5, 1994.

[11] Araki, M., "Recent developments in digital control theory," *Twelfth IFAC world congress*, Vol. 9, pp. 251-260, 1993.

[12] Arimoto, S., S. Kawanura, F. Miyazaki, and S. Tamaki, "Learning Control Theory for Dynamical Systems," *Proc. 24th Conf. Decision and Control*, Ft. Lauderdale, FL, 1985, pp. 1375-1380.

[13] Bamieh, B. A. and J. B. Pearson, "The H_2 problem for sampled-data systems," *Systems and control letters*, vol. 19, pp. 1-12, 1992.

[14] Bamieh, B. A. and J. B. Pearson, "A general framework for linear periodic systems with applications to H_∞ sampled-data control," *IEEE Trans. Automat. Contr.*, vol. 37, no. 4, pp. 418-435, 1992.

[15] Banther, M., Y. Huang, and W. C. Messner, "Optimal strain gauge placement for an instrumented disk drive suspention," *Proc. 1998 American Control Conf.*, Jun. 1998, Philadelphia, PA, USA, pp. 3023-3027.

[16] Berger, C. S. and D. Peduto, "Robust digital control using multirate input sampling," *Int. J. Control*, Vol. 67, No.5, pp. 813-824, 1997.

[17] Berg, M. C., N. Amit, and J. D. Powell, "Multirate digital control system design," *IEEE Trans. Automat. Contr.*, Vol. 33, No. 12, pp. 1139-1150, 1988.

[18] Berg, M. C. and G. S. Mason, "New multirate sampled-data control law structure and synthesis algorithm," *Journal of Guidance , Control and Dynamics*, Vol.15, No. 5, pp. 1183-1191, 1992.

[19] Bodson, M., A. Sacks, and P. Khosla, "Harmonic generation in adaptive feedforward cancellation schemes," *IEEE Tran. Automatic Control*, Vol. 39, No. 9, pp. 1939-1944, September 1994.

[20] Bodson, M., J. S. Jensen, and S. C. Douglas, "Active noise control for periodic disturbances," *IEEE Trans. Contr. Sys. Tech.*, pp. 200-205, 2001.

[21] Brown, L. J. and Q. Zhang, "Periodic disturbance cancellation with uncertain frequency," *Automatica*, 40, pp. 631-637, 2004.

[22] Chen, B. M., T. H. Lee and V. Venkataramanan, "Hard disk drive servo systems," Springer, New York, 2002.

[23] Chen, B. M., T. H. Lee, C. C. Hang, Y. Guo and S. Weerasooriya, "An H_∞ almost disturbance decoupling robust controller design for a piezoelectric bimorph actuator with hysteresis," *IEEE Tran. Control Systems Technology*, Vol. 7, No. 2, pp. 160-174, 1999.

[24] Chen, D. and B. Paden, "Nonlinear adaptive torque-ripple cancellation for step motors," *Proc. 29th IEEE Conf. Decision and Control*, pp. 3319-3324, 1990.

[25] Chen, R., G. Guo, T. Huang, T. S. Low, and S. Weerasooriya, "Optimal multirate control design for embedded HDD servo systems," *IEEE Trans. Magnetics*, Vol. 34, No. 2, pp. 1898-1900, 1998.

[26] Chen, R., G. Guo, T. Huang, and T. S. Low, "Adaptive multirate control design for HDD servo systems," *IECON98, 24th annual conference of the IEEE Industrial Electronics Societies*, 1998, Aachen, Germany, Vol. 3, pp. 1716-1720.

[27] Chen, R., G. Guo, T. Huang, and T. S. Low, "Intersample ripple free multirate control design for HDD servo", *IECON99, 25th Annual Conference of the IEEE Industrial Electronics Societies*, San Jose, USA, 1999.

[28] Chen, T. and B. A. Francis, "H_2-optimal sampled-data control," *IEEE Trans. Automat. Contr.*, vol. 36, no. 1, pp. 50C58, 1991.

[29] Chen, T. and L. Qui, "H_infty design of general multi-rate sampled-data conrol system," *Proc. of 40th IEEE conf. on Decis. and Contr.*, pp. 4693-4698, 1994

[30] Chen, T. and B. A. Francis, "Design of multirate filter banks by H_∞ optimization," *IEEE Trans. Signal Processing*, vol. 43, pp. 2822-2830, 1995.

[31] Chew, K. K. and M. Tomizuka, "Digital control of repetitive errors in disk-drive systems," *IEEE Control Systems Magazine*, Vol. 10, No. 1, pp. 16-20, Jan. 1990.

[32] Chew, K. K., "Control system challenges to high track density magnetic disk storage," *IEEE Trans. Magnetics*, Vol. 32, No. 3, pp. 1799-1804, 1996.

[33] Chiang, W. W., "Multirate state-space digital controller for sector servo systems," *Proc. 19th IEEE Conf. Decision and Control*, Dec. 1990, Vol. 3, Honolulu, HI, USA, pp. 1902-1907.

[34] Dahleh, M. A., P. G. Voulgaris, and L. S. Valavani, "Optimal and robust controllers for periodic and multirate systems," *IEEE Trans. Automat. Contr.*, Vol.37, No. 1, pp. 90-99, 1992.

[35] Draijer, W., M. Steinbuch, and O. Bosgra, "Adaptive Control of the Radial Servo System of a Compact Disc Player," *Automatica*, Vol. 28, No. 3, pp. 455-462, 1992.

[36] Enrlish, R., J. Adler, and H. Hindi, "Rejecting oscillatory non-synchronous mechanical disturbances in hard disk drives," *IEEE Trans. on Magnetics*, Vol. 37, Part: 1, pp. 646 -650, March, 2001.

[37] Feng, L., W .E .Wong, G. Guo, Z. He, C. Duan, and T. C. Chong, "Stretching the servo performance on a spin stand," *Proc. American Control Conf.*, Jun 30 - July 2, 2004, Boston, Massachusetts, pp. 1159-1164

[38] Francis, B. and B. Wonham, "The internal model principle of control theory," *Automatica*, Vol. 12, No. 5, 1976, pp. 457-465.

[39] Franklin, G. F., J. D. Powell, and M. L. Workman, *Digital control of dynamic systems*, 2nd edition, Addison-Wesley Publishing Company, Reading, MA, 1990.

[40] Franklin, G. F., J. D. Powell, and A. Emami-Naeini, *Feedback control of dynamic systems*, 3rd edition, Addison-Wesley Publishing Company, Reading, MA, 1994.

[41] Fujimoto, H., Y. Hori, T. Yamaguchi, and S. Nakagawa, "Proposal of perfect tracking and perfect disturbance rejection control by multirate sampling and applications to hard disk drive control," *Proc. of the 38th IEEE Conference on Decision and Control*, Vol. 5, pp. 5277-5282, 1999.

[42] Fujimoto, H., Y. Hori, A. Kawamura, "Perfect tracking control based on multirate feedforward control with generalized sampling periods," *IEEE Tran. Ind. Elec.*, pp. 636-644, 2001.

[43] Fujimoto, H., Y. Hori, "High-performance servo systems based on multirate sampling control," *Control Engineering Practice*, pp. 773-781, 2002.

[44] Fujita, H., K. Suzuki, M. Ataka, and S. Nakamura, "A microactuator for head positioning system of head disk drives," *IEEE Trans. on Magnetics*, Vol. 35, pp. 1006-1010, 1999.

[45] Glasson, D. P., "Development and applications of multirate digital control," *IEEE Control Sys. Magazine*, pp. 2-8, 1983.

[46] Godbout, L. F., D. Jordan, and S. Apostolakis, "Closed-Loop model for general multirate digital control systems," *IEE Proc.*, Vol.137, Pt. D, No. 5, pp. 329-336, 1990.

[47] Goodwin, G. C. and R. M. Ehrlich, "Frequency viewpoint of multirate control," *Proc. American Control Conference*, pp. 4156-4160, June, 1993.

[48] Grochowski, E., "Emerging trends in data storage on magnetic hard disk drives," *Datatech*, pp. 11-16

[49] Guo G., Y. Wang, K.-Y. Lim, and L. Gao, "Robust nonlinear controller for power systems transient stability enhancement with voltage regulation," *IEE Proc.*, Pt. C, Vol. 143, pp. 407-412, 1996.

[50] Guo, G., R. Chen, T. S. Low, and Y. Wang, "Optimal control design for hard disk drive servo systems," *IEE Proc. Control Theory and Applications*, Vol 149, pp. 237-242, May 2002.

[51] Guo, G., *Servo engineering- part II, hard disk drive actuator servo control*, Lecture Notes, National University of Singapore, 2004.

[52] Guo, G., T. Huang, K. M. Tay, S. Weerasooriya, and A. Al-Mamun, "A DSP based hard disk drive servo test stand," *IEEE Trans. on Magnetics*, Vol. 34, No. 2, pp. 480-482, 1998.

[53] Guzik Company Website [Online], Spin Stand Products Information, *http://www.guzik.com.*

[54] Hara, S., Y. Yamamoto, T. Omata, and M. Nakano, "Repetitive control system: a new type servo system for periodic exogenous signals," *IEEE Tran. Automatic Control*, Vol. 33, No. 7, pp. 659-668, July 1998.

[55] Hara, T. and M. Tomizuka, "Multi-rate controller for hard disk drive with redesign of state estimator," *Proc. 1998 American Control Conf.*, Jun. 1998, Philadelphia, PA, USA, pp. 3033-3037.

[56] Hara, T. and M. Tomizuka, "Performance enhancement of the multirate controllers for hard disk drives," *IEEE Trans. Magnetics*, Vol. 35, No. 2, pp. 898-903, 1999.

[57] Hayakawa, Y., S. Hara, and Y. Yamamoto, "H_∞ type problem for sampled-data control systems - a solution via minimum energy characterization," *IEEE Trans. Automat. Contr.*, vol. 39, no. 11, pp. 2278-2284, 1994.

[58] Hirata, M., M. Takiguchi, and K. Nonami, "Track-following control of hard disk drives using multi-rate sampled-data H_infty control," *Proc. of the IEEE conf. on Contr. and Decis.*, pp. 3414-3419, Maui, 2003

[59] Horowitz, R. and B. Li, "Adaptive tracking-following servos for disk file actuators," *IEEE Trans. on Magnetics*, Vol. 32, No. 3, pp. 1779-1786, 1996.

[60] Horowitz, R. and Y. Li, "Active suspension vibration control with dual stage actuators in hard disk drives," *Proc. ACC'01*, pp. 2786-2791, Arlington, VA, USA, 2001.

[61] Hospodor, A. D. and A. S. Hoagland, "The changing nature of disk controllers," *Proc. of the IEEE*, Vol. 81, No. 4, pp. 586-594, April, 1993.

[62] Huges, E. C. and W. C. Messner, "Characterization of three servo patterns for Position Error Signal Generation in Hard Drives," *Proc. American Control Conf.*, pp. 4317-4322, Jun. 2003.

[63] Ioannou, P. A. and G. Tao, "Frequency domain conditions for strictly positive real functions," *IEEE Tran. Automatic Control*, vol. AC-32, No. 1, pp. 53-54,1987.

[64] Jia, Q. W., F.C Cai, and Z. F. Wang, "A new RRO data collection method for HDD," *Digest of the Asia Pacific Magnetic Recording Conf. 2004, APMRC'04*, SV02-1, 2, Seoul, Korea, Aug. 17-19, 2004.

[65] Kabamba, P. T. and S. Hara, "Worst-case analysis and design of sampled-data control systems," *IEEE Trans. Automat. Contr.*, vol. 38, no. 9, pp. 1337-1357, 1993.

[66] Kalman, R. E. and J. E. Bertram, "A unified approach to the theory of sampling systems," *J. Franklin Inst.*, Vol. 267, pp. 405-436, May, 1959.

[67] Kempf, C., W. Messner, M. Tomizuka, R. Horowitz, "Comparison of four discrete-time repetitive control algorithms," *Proc. Amer. Contr. Conf.*, pp. 2700-2704, 1992.

[68] Kranc, G. M., "Input-Output analysis of multirate feedback systems," *IRE Trans. Automat. contr.*, Vol. 2, pp. 21-28, Nov., 1957.

[69] Lee, S. H., C. C. Chung, and S. M. Suh, "Multirate digital control for high track density magnetic disk drives" *IEEE Trans. Magn.*, pp. 832-837, 2003.

[70] Li, Y. and M. Tomizuka, "Two-Degree-of-Freedom control with robust feedback control for hard disk servo systems" *IEEE/ASME Trans. Mechatron.*, pp. 17-24, 1999.

[71] Low, T. S., "Magnetic recording beyond 10 gigabits per square inch - the challenges in the mechatronics," *Professorial lectures for technology month 98*, National University of Singapore, pp. 45-75, 1998.

[72] Mee, C. D. and E. D. Daniel, *Magnetic storage handbook*, McGraw-Hill, 1987.

[73] Messner, W., R. Horowitz, W-W, Kao, M. Boals et.al, "A new adaptive learning rule," *IEEE Trans. Magn.*, pp. 188-197, 1991.

[74] Meyer, R. A. and C. S. Burrus, "A unified analysis of multirate and periodically time-varying digital filters," *IEEE Trans. Circuits and Systems*, Vol. 22, No. 3, pp. 162-168, 1975.

[75] Moore, K. L., S. P. Bhattacharyya, and M. Dahleh, "Capabilities and limitations of multirate control schemes," *Automatica*, Vol.29, No. 4, pp. 941-951, 1993.

[76] Niu, Y., W. Guo, G. Guo, E.-H. Ong, and T. Huang, "A piezoelectrically actuated suspension for hard disk drive," *IEEE Trans. on Magnetics*, Vol. 36, No. 5, pp. 2241-2243, Sep., 2000.

[77] Ohno, K., M. Hirata, and R. Horowitz, "A comparative study of the use of the generalized hold function for HDDs," *Proc. of the IEEE conf. on Contr. and Decis.*, pp. 5967-5972, Maui, 2003

[78] Ong, E. H., Z. He, R. Chen, G. Guo, and H. Qian, "A low turbulence high bandwidth actuator arm design," *IEEE Trans. on Magnetics*, Vol. 36, No. 5, pp. 2235-2237, Sep., 2000.

[79] Onuki, Y. and H. Ishioka, "Compensation for repeatable tracking errors in hard drives using discrete-time repetitive controllers" *IEEE Trans. Mechatron.*, pp. 132-136, 2001.

[80] Phan, D. T., "The design and modeling of multirate digital control systems for disk drive applications," *Proc. Asia-Pacific Workshop on Advances in Motion Contr.*, pp. 189-205, June, 1993.

[81] Physik Instrumente (PI) Company Website [Online], Piezo Products Information, *http://www.physikinstrumente.com/*

[82] Sacks, A., M. Bodson, and P. Khosla, "Experimental results of adaptive periodic disturbance cancellation in a high performance magnetic disk drive," *Proc. of the American Control Conf.*, San Francisco, California, June 1993, pp. 686-690.

[83] Sacks, A., M. Bodson, and W. Messner, "Advanced methods for repetitive runout compensation," *IEEE Trans. Magnetics*, Vol. 31, No. 2, pp. 1031-1036, 1995.

[84] Sklansky, J. and J. R. Ragazzini, "Analysis of errors in sampled-data feedback systems-Part II," *AIEE Trans.*, Vol. 74, pp. 65-71, Nov., 1955.

[85] Sri-Jayantha, S. M., H. Dang, A. Sharma, I. Yoneda, N. Kitazaki, and S. Yamamoto, "TrueTrack servo technology for high TPI disk drives" *IEEE Trans. Magn.*, pp. 871-876, 2001

[86] Tomizuka, M., "Zero phase error tracking algorithm for digital control," *J. Dynamic Systems, Measurement, Trans. of ASME*, Vol. 109, pp. 65-68, 1987.

[87] Weaver, P. A. and R. M. Enrlich, "The use of multirate notch filters in embedded-servo disk drives," *Proc. 1995 American Control Conf.*, Jun. 1995, Seattle, WA, USA, pp. 4156-4160.

[88] Weerasooriya, S., T. S. Low and J. L. Zhang, "An improved runout compensator," *Asia-Pacific Magnetic Recording Conference*, Singapore, 1995 (poster session)

[89] Weerasooriya, S., J. L. Zhang, and T. S. Low, "Efficient implementation of adaptive feedforward runout cancellation in a disk drive," *IEEE Trans. Magn.*, Vol.32, No. 5, pp. 3920-3922, 1996.

[90] Wittenmark, B. and K. J. Åström, "Practical issues in the implementation of self-tuning control," *Automatica*, Vol. 20, No. 5, pp. 595-605, 1984.

[91] Wong, W. E., G. Guo, A. Al-Mamun, W. Ye, and J. L. Zhang, "A position encoding and decoding scheme for ultra high density magnetic recording," *Proc. Asia Pacific Magnetic Recording Conference*, pp. WE-P-08, Aug 2002.

[92] Wu, D., G. Guo, and T.C. Chong, "Adaptive compensation of microactuator resonance in hard disk drives," *IEEE Trans. on Magnetics*, Vol. 36, No. 5, pp. 2247 - 2270, Sep., 2000.

[93] Wu, D., G. Guo and T. C. Chong, "Midfrequency disturbance suppression via Micro-Actuator in dual-stage HDDs," *IEEE Trans. Magn.*, pp. 2189-2191, 2002.

[94] Xu, J., T. H. Lee, and H. Zhang, "Comparative studies on repeatable runout compensation using iterative learning control," *proc. Amer. Contr. Conf.*, pp. 2834-2839, 2001.

[95] Yamada, K., S. Komada, M. Ishida, and T. Hori, "Analysis and classical control design of servo system using high order disturbance observer," *ACC'95.*, Vol. 1, pp. 4-9. Seattle, WA, 1995.

[96] Yamaguchi, T., K. Usui, and H. Hirai, "Modeling and TMR (Track Misregistration) budget design for head-positioning of high track-density disk drives," *IEEE Trans. Magnetics*, Vol. 35, No. 2, pp. 892-897, 1999.

[97] Yamaguchi, T. and S. Nakagawa, "Recent control technologies for fast and precise servo system of hard disk drives," *Proc. of 6th International Workshop on Advanced Motion Control*, pp. 69-73, Nagoya, Japan, 2000.

[98] Yamamoto, Y., H. Fujioka, and P. P. Khargonekar, "Signal reconstruction via sampled-data control with multirate filter banks," *Conf. Decision Contr.*, pp. 3395-3400, 1997.

[99] Yamaura, H. and M. Tomizuka, "A new design method for discrete equivalents of analog controllers," *Proc. American Control Conf.*, Vol. 3, pp. 1986 -1992, Chicago, IL, USA, 2000.

[100] Yang, H. S., J. Jeong, C. H. Park, adn Y. P. Park, "Identification of contributors to HDD servo errors by measuring PES only," *IEEE Tran. Magn.*, Vol. 37, pp. 883 - 887, 2001

[101] Zhang, J., Efficient implementation of repeatable runout compensation in a hard disk drive. Master Thesis, National University of Singapore. 1997

[102] Zhang, J., S. Weerasooriya, and T. S. Low, "Modified AFC Runout cancelation and its influence on track following," *Proc. IECON'97*, USA, pp. 35-40, 1997.

[103] Zhang, J., R. Chen, G. Guo, and T. S. Low, "Modified adaptive feedforward runout compensation for dual-stage servo system," *IEEE Trans. Magn.*, pp. 3581-3584, 2000.

[104] Duan, C., G. Guo, and T. C. Chong, "Robust periodic disturbance compensation via multirate control," *Digest of the Asia Pacific Magnetic Recording Conf. 2004, APMRC'04*, SV03-1, 2, Seoul, Korea, Aug. 17-19, 2004. The full paper has been submitted to IEEE. Trans. on Mechatron.